iTAP, a novel iRhom interactor, controls TNF secretion by policing the stability of iRhom/TACE

iTAP, a novel iRhom interactor, controls TNF secretion by policing the stability of iRhom/TACE

Ioanna Oikonomidi[1], Emma Burbridge[1], Miguel Cavadas[1], Graeme Sullivan[2], Blanka Collis[6], Heike Naegele[7], Danielle Clancy[2], Jana Brezinova[6], Tianyi Hu[1], Andrea Bileck[4,5], Christopher Gerner[4], Alfonso Bolado[3], Alex von Kriegsheim[3], Seamus J. Martin[2], Florian Steinberg[7], Kvido Strisovsky[6], Colin Adrain[1].

1, Membrane Traffic Lab, Instituto Gulbenkian de Ciência (IGC), Oeiras, Portugal
2, Molecular Cell Biology Laboratory, Department of Genetics, The Smurfit Institute, Trinity College, Dublin 2, Ireland.
3, Edinburgh Cancer Research UK Centre, Institute of Genetics and Molecular Medicine, University of Edinburgh, Edinburgh, UK.
4, Institut für Analytische Chemie, Universität Wien, Wahringer Strasse 38, 1090 Vienna, Austria.
5, Present address: Department of Clinical Research, Department of Nephrology and Hypertension, Bern University Hospital, University of Bern, Bern, Switzerland.
6, Institute of Organic Chemistry and Biochemistry, Academy of Sciences of the Czech Republic, Flemingovo n. 2, Prague, 166 10, Czech Republic.
7, Center for Biological Systems Analysis (ZBSA), Faculty of Biology, Albert Ludwigs Universitaet Freiburg, Freiburg, Germany.

Correspondence and lead contact: cadrain@igc.gulbenkian.pt

Running title.
iTAP controls stability of iRhom2 and TACE.

Abstract. (150 words max)
The apical inflammatory cytokine TNF regulates numerous important biological processes including inflammation and cell death, and drives inflammatory diseases. TNF secretion requires TACE (also called ADAM17), which cleaves TNF from its transmembrane tether. The trafficking of TACE to the cell surface, and stimulation of its proteolytic activity, depends on membrane proteins, called iRhoms. To delineate how the TNF/TACE/iRhom axis is regulated, we performed an immunoprecipitation/mass spectrometry screen to identify iRhom-binding proteins. This identifies a novel protein, that we name iTAP (iRhom Tail-Associated Protein) that binds to iRhoms, enhancing the cell surface stability of iRhoms and TACE, preventing their degradation in lysosomes. Depleting iTAP in primary human macrophages profoundly impaired in TNF production and tissues from iTAP KO mice exhibit a pronounced depletion in active TACE levels. Our work identifies iTAP as a physiological regulator of TNF signalling and a novel target for the control of inflammation.

Key words: ADAM17/TACE; iRhom; vesicular trafficking; iTAP, FRMD8; TNF; EGFR

Introduction

The cytokine TNF controls numerous important biological processes (e.g. inflammation, fever, apoptosis, necroptosis, cachexia, tumorigenesis, viral infection, insulin signaling) and is heavily implicated in inflammatory disease[1]. Anti-TNF biologics are the highest-selling drugs internationally and there is intense interest in how TNF signaling is regulated[1]. TNF is expressed by a range of cells including macrophages, lymphocytes, natural killer cells, endothelial cells and microglia and is synthesized as a type II transmembrane protein with a cytosolic domain of 76 amino acids that assembles into a trimer[2]. The capacity of TNF to trigger such pleiotropic biological outcomes is determined by its ability to activate two distinct receptors[2]. Generally, TNFRI activation is associated with induction of acute or chronic inflammatory responses, or cell death, whereas TNFRII mediates pro-survival signals and has been associated with the tolerogenic properties of regulatory T cells[3,4].

Additional complexity is imposed by the form of TNF that engages in signalling. The transmembrane form of TNF (mTNF) triggers juxtacrine signalling, while TNF released as a soluble form (sTNF), drives paracrine signalling. Notably, whereas TNFRI can be activated by both soluble and membrane TNF, TNFRII is activated efficiently only by mTNF[5]. Whereas mTNF is sufficient for the development and maintenance of some lymphoid tissues, soluble TNF is important for acute and chronic inflammation. Specifically, mice unable to produce soluble TNF resist endotoxic shock and exhibit reduced severity in experimental autoimmune encephalomyelitis models[6]. Membrane TNF is also insufficient to rescue the defects in primary B cell follicle formation observed in TNF KO mice, but mediates protective immune responses to intracellular bacterial infection[6,7].

The ability to engage biological outcomes that require TNFRI versus TNFRII, (and the capacity to control the physical distance over which signaling is effective) therefore, critically depends on the ability to release soluble TNF from the cell surface. This is catalyzed by the protease TACE (TNF α Converting Enzyme)[8,9], also called ADAM17 (A Disintegrin And Metalloprotease)[10,11]. Crucially, TACE imposes an additional layer of versatility and regulation to TNF signaling, since in addition to cleaving TNF, both TNFRs are also physiological TACE substrates. Hence, TACE is a master orchestrator of TNF signaling, tuning signaling to fit a panoply of biological roles ranging from inflammatory responses to immune tolerance. TACE also has significant biological importance beyond TNF signaling since it cleaves other prominent substrates, including the activating ligands of the EGFR (Epidermal Growth Factor Receptor), an important pathway that drives growth control, tissue repair and immune responses.

Given its ability to elicit potent biological responses, it is unsurprising that TACE is stringently regulated[12,13]. A major control point in TACE regulation involves its trafficking within the secretory pathway[14]. TACE is synthesized in the endoplasmic reticulum (ER) as a catalytically inactive precursor. For TACE to become proteolytically active, it must undergo a maturation step—removal of its prodomain—which is catalysed by proprotein convertases in the *trans*-Golgi[14]. The exit of TACE from the ER and its trafficking to the cell surface requires regulatory proteins called iRhoms[15–17]. Hence, iRhom KO mice, or cells in which iRhoms are ablated, lack TACE

activity[15,17,18]. Mice null for iRhom2, whose expression is enriched in myeloid cells, cannot secrete TNF[15,16,19].

An important checkpoint to license TACE activity involves its stimulation on the cell surface by agents including phorbol esters, Toll-like receptor agonists and G-protein coupled receptor ligands[13,20–23]. Importantly, as well as controlling TACE trafficking, iRhoms exist in a molecular assembly with TACE on the cell surface—the "sheddase complex" which is central to stimulation of TACE sheddase activity. Within the sheddase complex, iRhom proteins serve as a platform that senses and transduces TACE-activating stimuli. These agents provoke the MAP kinase-dependent phosphorylation of the iRhom2 cytoplasmic tail, which in turn triggers the recruitment of 14-3-3 proteins. This enforces the detachment of TACE from iRhom2 (or triggers a conformational change within the sheddase complex) which is required to facilitate TACE's ability to cleave its substrates, including TNF[24,25]. Hence, iRhoms are allosteric regulators of TACE's proteolytic activity as well as acting as trafficking factors.

As iRhom and TACE form an intrinsic complex, their trafficking itinerary and fate within the secretory pathway must presumably be interdependent. In spite of the importance of trafficking for TACE regulation[14,15,26], surprisingly little is known about the machinery that controls TACE, or iRhom, trafficking to/from the plasma membrane. An exception is PACS-2 (Phosphofurin Acidic Cluster Sorting Protein 2), a protein that colocalizes with mature TACE in endocytic compartments[26] and controls its endocytic recycling. Ablation of PACS-2 in cells impairs the cell surface availability of TACE, reducing substrate cleavage[26]. However, PACS-2 has a relatively modest impact on TACE biology *in vivo*[27], suggesting the possibility of unidentified trafficking regulators that may act separately from, or redundantly with, PACS-2.

As iRhoms form functionally important complexes with cell surface TACE[24,25,28], modulation of iRhom trafficking in the endocytic pathway has the potential to act as a regulatory mechanism that controls TNF secretion. It has been shown that not only TACE[29,30], but also iRhoms[24,25] are endocytosed and degraded in lysosomes, but the machinery involved in maintaining stable cell surface levels of the sheddase complex is unknown.

Here we identify a novel protein that we name iTAP (iRhom Tail-Associated Protein) that is essential for the control of the stability of iRhom2 and TACE on the plasma membrane. Ablation of iTAP triggers the mis-sorting of iRhom2, and consequently, TACE, to lysosomes, where they are degraded. Consistent with this, loss of iTAP results in a dramatic reduction in TACE activity and TNF secretion. Our work reveals iTAP as a key physiological regulator of TNF release.

Results

iTAP, a novel interactor of iRhoms, is an atypical FERM domain-containing protein.

To identify novel regulators of mammalian iRhoms 1 and -2, we adopted an immunoprecipitation/mass spectrometry (IP/MS) approach described in our previous work[25]. As shown in Figure 1A, we generated a panel of HEK 293ET cell lines stably expressing HA-tagged forms of full-length iRhom1, iRhom2, or the iRhom1 N-terminal cytoplasmic tail only. To focus only on

proteins that bind selectively to iRhoms, we included the related rhomboid-like proteins, Rhbdd2, RHBDD3, Ubac2, as specificity controls (Figure 1A). As expected, only immunoprecipitates (IPs) from cells expressing full-length HA-tagged iRhom1 or iRhom2 captured endogenous TACE, confirming the validity of the approach (Figure 1B).

To identify novel iRhom-binding proteins, we subjected IPs from these cells to mass spectrometry. This analysis revealed, in multiple replicate experiments, peptides from a largely uncharacterized protein, called FRMD8 (FERM Domain-containing protein 8), in IPs of iRhom1 or iRhom2, but not in control IPs of Rhbdd2, RHBDD3 and Ubac2 (Figure 1C). Furthermore, FRMD8 was found in IPs from cells expressing the N-terminus of iRhom1 (Figure 1A,C), suggesting that it was recruited to the iRhom cytoplasmic tail (R-domain), an important regulatory region[24,25,28,31]. In light of this, we named the novel protein iTAP ('iRhom Tail Associated Protein'). A closer inspection of the iTAP sequence revealed that it encodes a FERM (band 4.1/Ezrin/Radixin/Moesin) domain[32] (Figure 1D).

Proteins containing FERM domains fulfil many important roles, including signaling, organization of the cell cortex and its mechanical properties and cell surface stabilization (anchoring) of membrane proteins or phospholipids[33–37]. The well-characterized FERM domain contains three distinct lobes that together resemble a three-leaf clover[38]. However, unlike most FERM domain-containing proteins, but similar to its paralog KRIT1—an adaptor protein in the cerebral cavernous malformation pathway that regulates the establishment of vasculature[39], iTAP contains only the central (FERM-M) lobe (Figure 1D). iTAP orthologs are present in metazoans, including *Drosophila* and *Danio*[40]. The iTAP protein is expressed broadly and is co-expressed with TACE and iRhom1 or iRhom2 in a range of tissues relevant for TACE biology (Figure 1—figure supplement 1A,B).

Independent immunoprecipitation experiments verified that iTAP binds specifically to both iRhom1 and iRhom2, but not to the related rhomboid pseudoproteases Ubac2 and Rhbdd2 (Figure 2A). iTAP binds the cytoplasmic tail of iRhoms, since a mutant containing only the cytoplasmic tail of iRhom1 bound iTAP robustly, whereas a mutant lacking all of the iRhom2 cytoplasmic tail (ΔNterm) failed to bind (Figure 2A). By contrast, removal of the iRhom homology domain (IRHD), the luminal globular domain between transmembrane helices 1 and 2 (Figure 2B) from iRhom2 had no impact on iTAP recruitment (Figure 2A). These data indicate that iTAP is specifically recruited to the cytoplasmic tail of iRhoms. Notably, when iTAP-FLAG, but not a panel of control proteins, was immunoprecipitated from cell lysates, we detected the binding of endogenous iRhom1 and iRhom2 to iTAP (Table 1). These data confirm that iTAP is a specific endogenous interactor of both iRhom paralogs in mammals.

To delineate the region within the cytoplasmic tail of iRhom that iTAP binds to, we divided the cytoplasmic tail into subdomains (Figure 2B) and, initially, created a series of sequential truncations within the iRhom2 cytoplasmic tail (Figure 2C). Then, we created more focussed deletions within the area identified in the previous experiment (Figure 2D). This revealed that amino acids 191-271 of the iRhom2 tail contain the main determinant for iTAP binding (Figure 2C,D). Further studies are required to assess whether the specific binding of iTAP to iRhom is direct, or via an intermediary.

We next examined the cellular localization of GFP-tagged iTAP in fixed and permeabilized mammalian cells. As shown in Figure 2—figure supplement 1A, iTAP-GFP exhibited a powdery

staining in the cytoplasm and nucleus. When co-expressed with mCherry-tagged iRhom2, iTAP was recruited to areas of iRhom2 staining (Figure 2—figure supplement 1B).

iTAP-deficient cells are impaired in the shedding of TACE substrates.

To determine the functional importance of iTAP binding to iRhom, we used CRISPR to ablate iTAP in HEK 293ET cells, which was confirmed by the lack of iTAP protein expression (Figure 3A). As TACE trafficking and cell surface stimulation depends on iRhoms, we examined the ability of WT versus iTAP-null cells to support release of TACE substrates. Notably, the PMA-induced shedding of a panel of chimeric alkaline phosphatase (AP) TACE substrates[41], including EGFR ligands and TNF, was substantially impaired in iTAP KO cells (Figure 3B). This shedding defect was rescued by the expression of an iTAP cDNA, confirming that the loss of iTAP was directly responsible for defective TACE activity (Figure 3C,D). To test the hypothesis that the basis for the shedding defects was in fact reduced TACE proteolytic activity in iTAP KO cells, we assayed TACE enzymatic activity directly using a peptide substrate (Figure 3—figure supplement 1). As expected, TACE immunoprecipitates (Figure 3—figure supplement 1A) from iTAP KO cells exhibited substantially depleted levels of TACE activity (Figure 3—figure supplement 1B), confirming that the loss of iTAP specifically impairs TACE rather than affecting its substrates.

Our previous studies have shown that iRhom proteins are highly specific regulators of TACE that do not affect the trafficking/activity of related proteases in the ADAM metalloprotease family, including ADAM10, the closest relative of TACE[15,18]. To examine whether iTAP was similarly dedicated specifically to the iRhom/TACE pathway we examined whether cleavage of the EGFR ligands EGF and BTC, which are cleaved specifically by ADAM10[41], was affected by loss of iTAP. Notably the cleavage of these ADAM10 substrates was unaffected (Figure 3E) while the release of a model secreted substrate was similarly unimpaired in iTAP KO cells (Figure 3F). These data confirm that iTAP is a highly specific regulator of the TACE pathway that does not affect secretion in general.

Mature TACE is specifically reduced in iTAP-deficient cells.

To investigate how loss of iTAP affected TACE so profoundly, we examined the maturation status of TACE, a readout for its trafficking and activation status[15] in iTAP KO cell lines (Figure 4A). As a positive control, we included lysates from iRhom1/iRhom2 double knockout MEFs which completely lack mature TACE[18]. Although a few experiments showed an overall reduction in the TACE levels in iTAP KO cells, the consistent and most pronounced phenotype, found in all iTAP-null cell lines, was a dramatic depletion of mature TACE, identified by its faster migration pattern (Figure 4B). As TACE is heavily glycosylated, to confirm this observation more clearly, we treated lysates with the deglycosylating enzymes Endoglycosidase-H (Endo-H), which removes high mannose N-linked glycans added in the ER, but not complex N-linked glycans found in the later secretory pathway, versus PNGase F, which deglycosylates both (Figure 4C,D). This confirmed that iTAP KO cell lines were substantially depleted of mature TACE (Figure 4B,D,E), which could be rescued specifically by iTAP overexpression in iTAP KO cells (Figure 4E). Overexpression of iTAP in WT cells also modestly

enhanced mature TACE levels (Figure 4E) and densitometric analysis confirmed once again that the loss, or reintroduction, of iTAP most profoundly affected mature TACE levels (Figure 4E, graphs).

A clear prediction from these experiments is that iTAP-null cells should lack mature, cell surface TACE, explaining the basis of the proteolytic defects observed (Figure 3, Figure 3—figure supplement 1A,B). We tested this hypothesis in experiments with a non-cell permeable biotinylated cross-linker, which revealed drastically reduced mature TACE levels on the cell surface (Figure 4F). Finally, as predicted by stringent specificity of iTAP for TACE, the maturation of other related ADAM proteases was unimpaired (Figure 4G). Together these data confirm that iTAP is a dedicated regulator of the iRhom/TACE sheddase complex.

iTAP is required to maintain iRhom2 stability in the late secretory pathway.

The observation that iTAP-null cells exhibited drastically depleted mature TACE levels could be explained by two potential mechanisms. First, loss of iTAP, which binds to iRhom2 (Figures 1-2; Table 1), could impair ER exit of the iRhom/TACE complex, causing a failure in TACE maturation, as observed in iRhom KO cells[15,18]. Alternatively, as TACE undergoes constitutive recycling from the plasma membrane[42] and iRhom2 traffics to the cell surface and enters the endolysosomal pathway[24,25,28], iTAP could stabilize iRhom/TACE complexes on the plasma membrane or within the endocytic pathway. Given the established role of FERM domain proteins in stabilizing proteins on the cell cortex, this second possibility seemed plausible.

To investigate the impact of iTAP on iRhom2 stability, we first used RAW 264.7 cells. These macrophage-like cells express high levels of endogenous iRhom2, making its detection more feasible than in HEK 293ET cells or MEFs. Strikingly, endogenous iRhom2 was depleted in iTAP KO RAW 264.7 cells (Figure 5A), indicating that iTAP is essential to maintain iRhom2 stability. Consistent with this, in HEK 293ET cells, iTAP transient overexpression increased steady state levels of overexpressed iRhom2-HA and enhanced the half-life (see graph, Figure 5B) of the protein, during a timecourse of cycloheximide (CHX) treatment, used to block additional protein synthesis (Figure 5B). This experiment, in which iRhom2 was expressed from an artificial promoter, indicates that the impact of iTAP on iRhom2 levels is independent of transcription. As anticipated by these results, transiently overexpressed iRhom2-HA was also destabilized in iTAP KO cells (Figure 5—figure supplement 1A). Consistent with the ability of iTAP to impact profoundly on iRhom2 stability, we observed striking colocalization between mCherry-iRhom2 and iTAP-GFP, when they were co-expressed in HeLa cells, as judged by Pearson's correlation and Manders' overlap coefficients (Figure 5C).

These colocalization data indicate that iRhom and iTAP interact in multiple compartments (Figure 5C), including the ER and plasma membrane. Two major possibilities exist to explain the decreased half-life of iRhom2 in iTAP KO cells: in the absence of iTAP, iRhom2 may be degraded in the early secretory pathway (the ER), or in the late secretory pathway (lysosomes). To address this, we used Endo-H deglycosylation to discriminate between the impact upon iTAP overexpression on the Endo-H-sensitive pool of iRhom2 in the ER, versus the Endo-H-insensitive fraction that has entered the later secretory pathway. As anticipated[43], most overexpressed iRhom2 is Endo-H sensitive, hence still located within the early secretory pathway (Figure 5D). Strikingly, the co-

expression of iTAP increased the overall levels of iRhom2, but selectively enriched the post-ER fraction of iRhom2 (Figure 5D), suggesting a disproportionate impact on the form of iRhom2 that had traversed to the late secretory pathway.

To obtain additional insights, we used a binding assay, coupled to deglycosylation analysis, to compare which species of iRhom2 bind to iTAP. Cells were treated with or without DSP, a thiol-reducible cell-permeable cross-linker, to covalently trap complexes *in situ*[15], enabling us to discriminate between interaction *in vivo*, compared to potential adventitious binding post-lysis. After immunoprecipitation, samples were treated with DTT to reverse the cross-linking. Notably, compared to IPs done without cross-linking, iTAP IPs from cross-linked cells showed a clear enrichment for post-ER (Endo-H insensitive) iRhom2 (Figure 5E), although the ER-localized form of iRhom2 was also readily detected. Taken together with the colocalization data (Figure 5C), we propose that the loading of iTAP onto the sheddase complex occurs already in the ER but the binding is sustained throughout the sheddase complex's itinerary in the late secretory pathway, where iTAP's affinity for iRhom2 appears to be higher. These data are consistent with the finding that iTAP selectively affects mature TACE (Figure 4). Finally, ruling out a requirement for iTAP in controlling the ER-to-Golgi trafficking of iRhom2, we found that the ER exit of iRhom2 was unimpaired in iTAP KO cells, judged by the presence of Endo-H-resistant iRhom2 (Figure 5F; Figure 5—figure supplement 1B). Hence, although iTAP binds to the sheddase complex in the early secretory pathway, its impact appears to be more decisive in the late secretory pathway.

iTAP modulates the plasma membrane stability of iRhom2 and TACE by preventing their aberrant sorting to the lysosome.

As ablation of iTAP results in dramatically reduced iRhom2 levels (Figure 5A) and iTAP increases the abundance of post-ER iRhom2 (Figure 5D,E), we hypothesized that iTAP controls the stability of iRhom2 in the late secretory pathway. Consistent with this premise, cell surface biotinylation experiments revealed that iTAP expression increased the steady state levels of cell surface iRhom2, and prolonged its cell surface stability, when CHX was used to block additional protein synthesis (Figure 5G). In further agreement, the co-expression of iTAP with GFP-iRhom2 in MEFs enhanced the amount of GFP-iRhom2 detected on the plasma membrane (Figure 5H), supporting the premise that iTAP promotes the cell surface stability of iRhom2. Together, our data indicate that iTAP's primary function is to stabilize the sheddase complex on the cell surface, reconciling the pronounced loss of mature TACE in iTAP KO cells and the increased binding propensity of iTAP for post-ER iRhom2.

We next addressed the functional basis for the pronounced loss of iRhom2 and mature TACE in iTAP KO cells. To test the hypothesis that loss of iTAP triggers the degradation of iRhom2 and TACE in lysosomes, the major degradative compartment in the late secretory pathway, we examined the localization of mCherry-iRhom2 in WT or iTAP KO HeLa cells derived by CRISPR (Figure 6—figure supplement 1). As shown in Figure 6A, in WT HeLa cells, mCherry-iRhom2 did not co-stain appreciably with lysosomes. By sharp contrast, iTAP ablation resulted in a pronounced co-localization of iRhom2 with the lysosomal marker LAMP2 (Lysosomal-Associated Membrane Protein 2), indicating

mis-sorting of iRhom2 to lysosomes. This phenotype was specific since the co-transfection of iTAP-GFP into iTAP KO HeLas rescued the aberrant accumulation of mCherry-iRhom2 in lysosomes (Figure 6B), resulting in the marked co-localization of iRhom and iTAP observed previously (Figure 2—figure supplement 1B; Figure 5C). Consistent with these observations, a panel of lysosomotropic drugs that inhibit lysosomal proteolysis by impairing lysosomal acidification, rescued iRhom2 stability in iTAP KO cells (Figure 6C).

The rescue of mature TACE under similar conditions was more modest (Figure 6D and data not shown), perhaps because of the slow trafficking time of TACE in the secretory pathway[14] and because iTAP acts directly on iRhoms. Consistent with the notion that iRhom2 can influence the routing of TACE into lysosomes, we found that overexpressed TACE-GFP was only recruited into lysosomes when sufficient iRhom2 was co-overexpressed (Figure 6E). In conclusion, our data reveal that when the normal stoichiometric ratio of iTAP to iRhom2 is disrupted (e.g. upon iRhom2 overexpression or iTAP ablation), iRhom2 is mis-sorted into the lysosome, then degraded. This highlights an important physiological role for iTAP in maintaining the cell surface stability of the iRhom2/TACE sheddase complex.

iTAP controls the stability of mature TACE, in mice.

iTAP is expressed in a range of mouse tissues relevant to iRhom and TACE biology[9,17] (Figure 1—figure supplement 1). As the experiments conducted so far focused on transformed cell lines, we next examined the physiological importance of iTAP at the organismal level. To examine the role of iTAP in mice, we generated a mutant in which the first coding exon (exon 2) of the *Frmd8* (iTAP) gene was deleted by CRISPR (Figure 7A, Figure 7—figure supplement 1). MEFs isolated from iTAP KO embryos lacked iTAP protein expression, confirming the successful targeting of the *Frmd8* gene (Figure 7B). As anticipated, MEFs from two independent iTAP KO embryos exhibited the characteristic pronounced depletion of mature TACE levels (Figure 7C).

Focussing next on potential phenotypes of the iTAP–null mouse mutants themselves, we harvested tissues from iTAP KO mice to assess the maturation status of TACE (Figure 7D). Significantly, with the possible exception of skin, where iTAP loss may be mitigated by other molecules, we observed a substantial depletion in the relative proportion of mature TACE in a range of iTAP KO mouse tissues, and in primary macrophages isolated from the bone marrow of iTAP KOs. These data reinforce the notion that iTAP is an important physiological regulator of the iRhom/TACE/TNF axis *in vivo,* making it important to dissect fully, in future, the organismal role of iTAP.

iTAP is a physiological regulator of TNF release in humans.

As the PMA-stimulated release of a chimeric alkaline phosphatase-tagged TNF was impaired in iTAP KO cells (Figure 3B), we hypothesized that iTAP was an important physiological regulator of TNF secretion. To test this, we isolated primary monocytes from peripheral human blood, then induced the differentiation of these cells to primary human macrophages. Notably, the stimulated release of endogenous TNF in response to lipopolysaccharide in these cells was profoundly impaired, when

iTAP expression was ablated by specific siRNAs (Figure 7E). As expected, secretion of IL-6 and IL-8, which is TACE-independent, was unaffected (Figure 7E). Our data indicate that iTAP is an essential physiological regulator of TNF secretion in primary human macrophages, the principal source of secreted TNF *in vivo*.

Discussion

Our work identifies iTAP as an important physiological regulator of the iRhom2/TACE sheddase complex, which is essential for the secretion of TNF and for a panoply of other substrates including ligands of the epidermal growth factor receptor. Our current and previous data[25] suggest that trafficking to, and degradation within, the lysosome is a default itinerary incurred by iRhom2, and that iRhom2 potentially encodes the determinants that lead to the default trafficking of iRhom2 and TACE to the lysosome. We now show that iTAP is essential to stabilize iRhom2 on the cell surface, preventing the routing of the sheddase complex to the lysosome, and licensing TACE to cleave its substrates for signaling (summarized in Figure 8). iTAP hence emerges as an important regulator of inflammation and growth factor signaling, during development, normal physiology, infection and inflammatory disease.

An obvious question concerns the extent to which the established features and roles of FERM domain proteins apply to iTAP and hence to the regulation of the iRhom/TACE pathway. A general theme is that FERM-domain proteins connect the cytoplasmic tails of cell surface client proteins to the cortical actin cytoskeleton, to enhance their stability[35–37]. While iTAP binds to the cytoplasmic tails of iRhoms, which are found on the plasma membrane, our preliminary experiments failed to detect robust binding of iTAP to actin (Figure 8—figure supplement 1A). Besides, we have not identified predicted actin binding motifs in the C-terminus of iTAP. Future experiments will be required to determine precisely how iTAP stabilizes iRhom and TACE in the late secretory pathway.

Some FERM-domain proteins are implicated in endosomal sorting, the process whereby endocytosed proteins are sorted in early endosomes, for routing to the multi-vesicular body, lysosome, *trans*-Golgi network, recycling endosome or alternatively, 'fast' recycling back to the cell surface[44]. Analogous to the degradation of iRhom2 in iTAP KO cells, loss of Snx17, which binds to the cytoplasmic tail of □1 integrins, results in a failure in their endocytic recycling, leading to their degradation in lysosomes[45]. Notably, the iRhom2 cytoplasmic tail contains two motifs, NxxY and NPxY (Figure 8—figure supplement 1B) that are the consensus endocytic signals recognized by a subset of FERM-domain proteins, sorting nexins, involved in endocytic recycling. However, our preliminary experiments in which we have mutated those motifs to alanines (AAAA), show that they appear not to be required for iTAP/iRhom2 binding (Figure 8—figure supplement 1C). Moreover, although sorting nexins are intimately connected with the endocytic recycling machinery, our preliminary experiments detect no obvious colocalization of iTAP with early endosomes (Figure 8—figure supplement 1D). Endocytic sorting is however only one theme within the wider FERM biology. Future studies will be required to clarify the relationship between iTAP and the trafficking machinery,

to map the vesicular itinerary taken by iRhom/TACE complexes, and to establish the precise basis of the mis-sorting defect in iTAP-null cells.

It will also be interesting to reconcile the role of iTAP in the control of iRhom/TACE stability, versus that of PACS-2, which binds directly to TACE[26]. iTAP and PACS-2 both impact on TACE stability, but iTAP can presumably only influence TACE stability indirectly via iRhoms. This is relevant because TACE stimulants trigger detachment of TACE from iRhom2 on the cell surface[24], a mechanism important for facilitating access of TACE to its substrates[25]. As iRhom and TACE are uncoupled at a crucial stage during signaling, their degradative fates could also be separated, leaving open the possibility that iTAP and PACS-2 may govern different stages in TACE's trafficking lifecycle.

The TNF (and EGFR) pathway(s) are very stringently regulated by positive and negative feedback[46–48]. Considering the significant impact that iTAP has on TACE biology, it is tempting to speculate that feedback control over the signaling pathways that culminate in TNF or EGFR ligand release, could be governed by controlling the interaction between iTAP and iRhom, or by modulating the stability of iTAP itself. Our preliminary experiments suggest that the phosphorylation of iRhom2 at residues required for the stimulation of TACE activity[25] does not appear to influence iTAP binding (data not shown), but future studies are required to investigate more widely the possibility of iTAP regulation by stimuli relevant to TACE biology.

In addition to our extensive evidence indicating the requirement for iTAP for normal TACE function in human and mouse cells, we show that mature TACE levels are dramatically depleted in tissues from iTAP KO mice, including macrophages (Figure 7D). This reinforces the notion that iTAP is an important physiological regulator of the sheddase complex at the organismal level, in multiple tissues. Notably, whereas ADAM17 homozygous mutant mice exhibit perinatal lethality[9], iTAP KO mice are born at near-normal mendelian ratios (Table 2), reach adulthood, appear superficially healthy and are fertile. These data indicate that although loss of iTAP indeed has a profound impact on the levels of mature TACE, the fraction remaining of mature TACE is sufficient to ensure normal mouse development.

Several hypomorphic TACE mutant mice have been studied, including *ADAM17*$^{ex/ex}$ mice, which were generated by the insertion of a new exon containing an in-frame stop codon, flanked by weak splice donor/acceptor sites inside the *Adam17* (TACE) locus[49]. 95% of the TACE mRNA produced contains the mutant exon, resulting in a dramatic reduction in TACE levels[49]. Notably, these animals are born at normal mendelian ratios but are highly susceptible when challenged to an experimental model of colitis[49]. This suggests that while traces of TACE can mitigate against lethality, they are not sufficient to prevent disease challenge. Hence, it will be important to dissect fully, in future, the organismal role of iTAP, particularly within the context of disease.

Inhibiting TACE activity has been the subject of considerable pharmaceutical interest for decades, but attempts have failed, often because of cytotoxicity caused by unintended collateral targeting of ADAMs and matrix metalloproteases, that share active site architectures related to TACE[50].

As iTAP has no apparent impact on other ADAMs, the blockade of the iRhom:iTAP interaction may be an interesting potential therapeutic approach to attenuate TACE activity during disease. Such

an approach would obviate the concern of collateral targeting of other metalloproteases. Although iTAP ablation at the cellular level has a potent impact on TACE substrate cleavage, at the organismal level the impact is significantly less severe than the lethal phenotype of TACE KO mice[9]. This implies that it may be possible to target iTAP to reduce TACE activity sufficiently to achieve a therapeutic impact in diseased tissues, without impinging on the normal physiological roles of TACE, which are sustained with minimal TACE levels in *ADAM17*$^{ex/ex}$ mutants[49] and presumably our iTAP KO mice.

Materials and Methods

Key Resources Table				
Reagent type (species) or resource	**Designation**	**Source or reference**	**Identifiers**	**Additional information**
gene (*Homo sapiens*)	*FRMD8*; iTAP, human	n/a	ENSG00000126391	
gene (*Mus musculus)*	*Frmd8*; iTAP, mouse	n/a	ENSMUSG00000024816	
strain, strain background (*Mm;* C57BL/6)	wild type; WT mice	Jackson Laboratories	RRID:IMSR_JAX:000664	
genetic reagent (*Mm*,C57BL/6)	iTAP KO mice	this paper	n/a	Generated by CRISPR (more details in M&M section and Figure 7—figure supplement 1)
cell line (*Hs*)	HEK 293ET	10.1038/sj.emboj.7601743	RRID:CVCL_6996	
cell line (*Hs*)	HeLa	ATCC	ATCC® CCL-2™; RRID:CVCL_0030	
Cell line (*Mm*)	RAW 264.7	Sigma	91062702; RRID:CVCL_0493	
Cell line (*Mm*)	L929	ATCC	ATCC® CCL-1; RRID:CVCL_0462	
cell line (*Hs*)	HEK 293ET iTAP KO	this paper	n/a	Generated by CRISPR (more details in M&M section)
Cell line (*Mm*)	RAW 264.7 iTAP KO	this paper	n/a	Generated by CRISPR (more details in M&M section)
Cell line (*Mm*)	L929 iTAP KO	this paper	n/a	Generated by CRISPR (more details in M&M section)
Cell line (*Mm*)	MEF iTAP KO	this paper	n/a	Isolated from iTAP KO mouse embryos
Cell line (*Mm*)	DKO MEF	10.1038/embor.2013.128.	n/a	Isolated from iRhom1/2 DKO mouse embryos
biological sample (*Mm*)	tissues from WT and KO mice	other	n/a	Isolated with standard techniques from the mice described here
antibody	anti-TACE; TACE Ab 318	https://doi.org/10.1016/j.jim.2011.06.015	n/a	
antibody	anti-TACE for Immunoprecipitation	R&D systems	R&D 9301	
antibody	anti-TACE	abcam	Ab39162; RRID:AB_722565	Ab39163
antibody	anti-P97	Thermo-Fisher	MA1-21412; RRID:AB_557663	
antibody	anti-TACE	R&D systems	9301; RRID:AB_2223551	
antibody	anti-TACE	10.1016/j.jim.2011.06.015	Ab318	monoclonal anti-TACE antibody[51] was used for the detection of deglycosylated TACE when no conA was used
antibody	anti-tubulin	IGC antibody facility	Clone YL1/2; RRID:AB_793541	

antibody	anti-HA-HRP	Roche	3F10; RRID:AB_2314622	
antibody	anti-HA	Biolegend	901501; RRID:AB_291259	
antibody	anti-V5-HRP	Life Technologies	R961-25	
antibody	anti-Frmd8	Abnova	157H00083786-B01P; RRID:AB_1573641	
antibody	anti-Transferrin Receptor	Life Technologies	13-6800; RRID:AB_2533029	
antibody	anti-Flag-HRP	Sigma	A8592; RRID:AB_439702	
antibody	anti-GAPDH	Cell signalling Technology	2118; RRID:AB_561053	
antibody	anti-actin	Abcam	Ab8227; RRID:AB_2305186	
antibody	anti-iRhom2	10.1126/science.1214400	n/a	Anti-iRhom2 polyclonal antibodies specific to the mouse iRhom2 N-terminus (amino acids 1-373) or raised against the iRhom homology domain, were previously described[15]
antibody	Anti-HA magnetic beads	Pierce	88836, Pierce	
antibody	Mouse anti-GFP	IGC antibody Facility	clone 19F7	Used as IP negative control in Figure 3—figure supplement 1
antibody	Anti-Flag M2 Affinity gel	Sigma	A220	
antibody	MagnaBind Goat Anti-Rabbit IgG Beads	Thermo Scientific	21356	
antibody	MagnaBind Goat Anti-Mouse IgG Beads	Thermo Scientific	21354	
antibody	mouse anti LAMP2	DSHB	Clone H4B4; RRID:AB_2134755	
antibody	rabbit anti EEA1	Cell signalling Technology	3288; RRID:AB_2096811	
antibody	rabbit anti Strumpellin/WASHC5	Santa Cruz	SC87442; RRID:AB_2234159	
Transfected construct (*Hs*)	h iRhom1-HA (plasmid)	this paper	n/a	
Transfected construct (*Hs*)	h iRhom1 Nterm HA (plasmid)	this paper	n/a	
Transfected construct (*Mm*)	Rhbdd2-HA (plasmid)	this paper	n/a	
Transfected construct (*Hs*)	RHBDD3-HA (plasmid)	this paper	n/a	
Transfected construct (*Mm*)	Ubac2-HA (plasmid)	this paper	n/a	
recombinant DNA reagent	pM6P.blast-GFP (plasmid)	Felix Randow	n/a	
recombinant DNA reagent	pLEX.blast (plasmid)	this paper	n/a	Details in M&M
Transfected construct (*Mm*)	mCherry-iRhom2 (plasmid)	doi:10.1038/ni.3510	n/a	
Transfected construct (*Hs*)	ADAM33-V5 (plasmid)	10.1038/embor.2013.128.	n/a	
Transfected construct (*Hs*)	ADAM19-V5 (plasmid)	10.1038/embor.2013.128.	n/a	
Transfected construct (*Hs*)	ADAM22-V5 (plasmid)	10.1038/embor.2013.128.	n/a	
Transfected construct (*Hs*)	ADAM8-V5 (plasmid)	10.1038/embor.2013.128.	n/a	
Transfected construct	TNF-FLAG (plasmid)	this paper	n/a	
Transfected construct (*Hs*)	STING-FLAG (plasmid)	doi:10.1038/ni.3510	n/a	
Transfected construct (*Hs*)	LAMP1-mCherry (plasmid)	this paper	n/a	Details in M&M
Transfected construct (*Mm*)	GFP-iRhom2 (plasmid)	this paper	n/a	Details in M&M
Transfected construct (*Mm*)	mCherry-iRhom2 (plasmid)	this paper	n/a	Details in M&M
Transfected construct (*Mm*)	TACE-GFP (plasmid)	this paper	n/a	Details in M&M
Transfected construct (*Mm*)	TACE-TagRFP (plasmid)	this paper	n/a	Details in M&M
Transfected construct (*Mm*)	mouse iTAP-mCherry (plasmid)	this paper	n/a	Details in M&M
Transfected construct (*Hs*)	human iTAP-GFP (plasmid)	this paper	n/a	Details in M&M

Transfected construct (*Mm*)	iRhom2 NPAY>AAAA (plasmid)	this paper	n/a	Quick change-based mutagenesis on iRhom2-HA plasmid described in M&M
Transfected construct (*Mm*)	iRhom2 NRSY>AAAA(plasmid)	this paper	n/a	Quick change-based mutagenesis on iRhom2-HA plasmid described in M&M
Transfected construct (*Mm*)	iRhom2 Double NxxY>AAAA(plasmid)	this paper	n/a	Quick change-based mutagenesis on iRhom2-HA plasmid described in M&M
Transfected construct (*Hs)*	SREBP2-FLAG (plasmid)	DOI: 10.1083/jcb.201305076	n/a	
recombinant DNA reagent	EGF-AP; EGF (plasmid)	doi: 10.1083/jcb.200307137	n/a	
recombinant DNA reagent	Betacellulin-AP; BTC-AP; BTC (plasmid)	doi: 10.1083/jcb.200307137	n/a	
recombinant DNA reagent	TNF-AP; TNF (plasmid)	doi: 10.1083/jcb.200307137	n/a	
recombinant DNA reagent	TGFα-AP; TGFα (plasmid)	doi: 10.1083/jcb.200307137	n/a	
recombinant DNA reagent	HB-EGF-AP; HB-EGF (plasmid)	doi: 10.1083/jcb.200307137	n/a	
recombinant DNA reagent	Epiregulin-AP; EPIREG-AP; EPIREG (plasmid)	doi: 10.1083/jcb.200307137	n/a	
recombinant DNA reagent	Amphiregulin-AP; AREG-AP; AREG (plasmid)	doi: 10.1083/jcb.200307137	n/a	
recombinant DNA reagent	secreted luciferase	10.1038/embor.2013.128.	n/a	
recombinant DNA reagent	Lenti-Crispr version2 (plasmid)	Addgene	52961	
recombinant DNA reagent	pLentiCas9-Blast(plasmid)	Addgene	52962	
recombinant DNA reagent	plentiGuide-Puro(plasmid)	Addgene	52963	
recombinant DNA reagent	pgRNAbasic(plasmid)	doi: 10.1242/dev.133074	n/a	
recombinant DNA reagent	pT7-Cas9(plasmid)	doi: 10.1242/dev.133074	n/a	
sequence-based reagent (siRNA; *Hs*)	iTAP oligo #1	Santa Cruz	sc-96500	
sequence-based reagent (siRNA; *Hs*)	iTAP oligo #2	GE Dharmacon	M-018955-01-0005	
sequence-based reagent (siRNA; *Hs*)	TACE oligo #1	Santa Cruz	sc-36604	
sequence-based reagent (siRNA; *Hs*)	TACE oligo #2	GE Dharmacon	M-003453-01-0005	
sequence-based reagent (CRISPR Guide sequence; *Hs;* cell lines)	gRNA targeting exon 1	this paper	n/a	5'-GCCCCGCTGAGCGATCCCAC-3'
sequence-based reagent (CRISPR Guide sequence; *Hs;* cell lines)	gRNA targeting exon 4	this paper	n/a	5'-ACGTGTTCTTCCCAAAGCGG-3'
sequence-based reagent (CRISPR Guide sequence; *Hs;* cell lines)	gRNA targeting exon 2	this paper	n/a	5'-TGACGTGCTGGTATACCTAG-3'
sequence-based reagent (CRISPR Guide sequence; *Hs;* cell lines)	gRNA targeting exon 6	this paper	n/a	5'-GGCACTTGAGGAGATAGGCG-3'
sequence-based reagent (CRISPR Guide sequence; *Mm; cell lines*)	gRNA targeting first exon	this paper	n/a	5'-TTCGGTGGGACCGCTCCGCA-3'
sequence-based reagent (CRISPR Guide sequence; *Mm; cell lines*)	gRNA targeting second exon	this paper	n/a	5'-GCACTACTGTATCATCCGCC-3'
commercial assay or kit	fluorogenic TACE substrate peptide	ENZO Life Sciences	BML-P235-0001	
commercial assay or kit	1-step PNPP Substrate	Thermo Fisher	PIER37621	
commercial assay or kit	Fugene 6	Promega	2691-SC	
commercial assay or kit	Endoglycosidase; Endo-Hf	NEB	174P0703	
commercial assay or kit	PNGase F	NEB	174P0704	
commercial assay or kit	Concanavalin A Agarose; conA	G-biosciences	786-216	

commercial assay or kit	MEGAshortscript T7 Kit	Thermo Fisher	AM1354	
commercial assay or kit	MEGAclear kit	Thermo Fisher	AM1908	
commercial assay or kit	Gibson Assembly Master Mix	New England Biolabs	174E2611	
commercial assay or kit	KOD Hotstart DNA polymerase	Novagen	71086-5	
commercial assay or kit	TOPO TA cloning kit for sequencing	Invitrogen	450030	
commercial assay or kit	mMESSAGE mMACHINE T7 Ultra Kit	Thermo Fisher	AM1345	
commercial assay or kit	human TNF ELISA kit	R&D Systems	DY210	
commercial assay or kit	human IL-6 ELISA kit	R&D systems	DY-206	
commercial assay or kit	human IL-8 ELISA kit	R&D systems	DY-208	
chemical compound, drug	Polyethylenimine; PEI	Sigma	408727	
chemical compound, drug	1,10-phenanthroline	Sigma	131377	
chemical compound, drug	Bafilomycin A1	Santa cruz	201550	
chemical compound, drug	Chloroquine	Sigma	C6628	
chemical compound, drug	Ammonium chloride	Acros	10676052	
chemical compound, drug	Ionomycin	Cayman	CAYM11932-5	
chemical compound, drug, (*E.coli 055:B5*)	Lipopolysaccharide ; LPS	Santa cruz	(sc-221855A)	
chemical compound, drug	Phorbol 12-myristate 13-acetate; PMA	Sigma	P1585	
chemical compound, drug	Cycloheximide; CHX	Santa cruz	sc-3508	
chemical compound, drug	Dithiobis (succinimidyl proprionate); DSP	Pierce	10731945	
chemical compound, drug	Sulfo-NHS-LC-Biotin	Thermo Scientific,	21335	
other	Lenti-X Concentrator	Clontech	Clonetech: 631231	
other	NeutrAvidin agarose; Neutravidin resin	Thermo Fisher	11885835	
other	NuPAGE Novex 4-12% Bit-Tris Protein Gels 1.0mm	Novex; Life Technologies	NP0322BOX	
other	Opti-MEM I Reduced Serum Medium, GlutaMAX	Life Technologies	51985-026	
software, algorithm	Fiji	PMID: 22743772	RRID:SCR_002285	
software, algorithm	Illustrator	Adobe	Adobe Creative Suite	
software, algorithm	GraphPad Prism	GraphPad Software, Inc.		
software, algorithm	Volocity	PerkinElmer		
software, algorithm	Geneious	Biomatters Ltd.	Javaversion 1.8.0_71-b15	
software, algorithm	perkin elmer 2030 workstation	PerkinElmer		

411

412

413 **Plasmids**

414 C-terminally triple HA-tagged versions of human iRhom1, the cytoplasmic N-terminus of iRhom1
415 (amino acids 1-404), mouse iRhom2, mouse Rhbdd2, human RHBDD3 and mouse Ubac2 were
416 cloned into the lentiviral expression plasmid pLEX-MCS, using Gibson cloning. These plasmids
417 were used only for the respective mass spectrometry experiments. C-terminally triple FLAG-
418 tagged iTAP and mouse iRhom2-HA were cloned into the retroviral pM6P vector (a kind gift of
419 Felix Randow) using Gibson assembly. The N-terminal truncations of iRhom2 used in Figure 2
420 were cloned into a modified version of the lentiviral expression vector pLEX-MCS in which the

puromycin resistance cassette was replaced with a blasticidin resistance gene. The packaging vectors for the production of retrovirus or lentivirus were described previously[25]. An mCherry-tagged iRhom2 plasmid previously described[52] was used only for the experiments in Figure 2—figure supplement 1. LAMP1-mCherry was subcloned from Addgene plasmid #45147 (a gift from Amy Palmer) into pM6P vector with zeocin resistance (prepared by replacing the blasticidin resistance gene in the original vector with zeocin resistance). Mouse GFP-iRhom2 and mouse TACE-GFP were cloned using Gibson assembly into pM6P.HisD vector. Mouse TACE-TagRFP was cloned using Gibson assembly into pM6P.Blast, using Addgene plasmid #42635 (a gift from Silvia Corvera) as a source of TagRFP DNA and a mTACE-GFP plasmid from Jürgen Scheller as a source of mTACE cDNA. Murine iTAP-mCherry (iTAP cDNA from Origene Technologies) and mCherry-iRhom2 were cloned using Gibson assembly into pM6P.Blast. Human iTAP was inserted with standard cloning techniques into the eGFP containing pIC111 vector (pIC111 is gift from Iain Cheeseman & Arshad Desai; Addgene plasmid # 44435). Alkaline phosphatase-tagged TACE substrates, a gift of Shigeki Higashiyama were described previously[41]. V5-tagged ADAM expression plasmids and secreted luciferase construct were described previously[18]. CRISPR plasmids are described below. Human Tumor Necrosis Factor (TNF) containing an N-terminal FLAG tag, was cloned into pCR3 by standard techniques. Flag-tagged SREBP2 was a gift of Larry Gerace and STING-FLAG a gift of Lei Jing). In figure 8—figure supplement 1C, iRhom2-HA in a modified version of pEGFP-N1/non EGFP was used as a template for Quick-Change mutagenesis resulting in the constructs iRhom2 NPAY>AAAA, iRhom2 NRSY>AAAA and iRhom2 Double NxxY>AAAA.

Cell culture

Our work involved the use of cell lines. Routine testing for mycoplama revealed mycoplasma negative status. None of our lines are identified on the list of commonly misidentified cell lines provided by ILCAC. We have noted the sources (eg ATCC accession number) of our lines in the Key resources table. HEK 293ET, RAW 264.7, L929, MEF and HeLa cell lines were maintained under standard conditions in Dulbecco's Modified Eagle Medium (DMEM)-high glucose supplemented with fetal bovine serum. Bone Marrow Derived Macrophages (BMDM) were isolated from 8-week old mice and cultured as previously described[15]. Embryonic fibroblasts were generated from E14.5 embryos and immortalized using lentiviral transduction of SV40 virus large T antigen.

Cytokine secretion in isolated human monocytes.

Primary human peripheral blood mononuclear cells (PBMC) were purified from donor whole blood using the Ficoll-Hypaque gradient method as described previously[53]. After overnight plastic adherence in heat-inactivated serum containing medium, non-adherent cells were removed and remaining cells were washed three times in PBS. Macrophage differentiation was induced using recombinant human macrophage-colony stimulating factor (M-CSF, 100 ng/ml) over five-seven days during cell culture in RPMI supplemented with 10% FCS. Primary human macrophages (5×10^5) were nucleofected with 200 nM of each siRNA (control NS oligo, MWG Eurofins - 5'-

GUUCCUGAGCCUGGACUAC -3'; iTAP oligo #1, Santa Cruz - catalog code sc-96500; iTAP oligo #2, GE Dharmacon - M-018955-01-0005; TACE oligo #1, Santa Cruz - sc-36604; TACE oligo #2, GE Dharmacon - M-003453-01-0005) in nucleofection buffer (5 mM KCl, 15 mM $MgCl_2$, 20 mM HEPES, 150 mM Na_2HPO_4 [pH 7.2]) using Amaxa Nucleofector (program Y-010). Cells were plated in 6-well plates (2 $\times 10^5$ cells/well) or in 24-well plates (1 $\times$ 10^5 cells/well) and 48 h after nucleofection were stimulated with lipopolysaccharide (LPS). After 18 h, cell culture supernatants were collected and clarified by centrifugation for 5 min at 800 x g. Cytokines and chemokine concentrations were measured from clarified cell culture supernatants using specific ELISA kits obtained from R&D Biotechne systems (human TNF – DY210; human IL-6 – DY206; IL-8 – DY208).

Retroviral transduction

HEK 293ET cells (1 x 10^6) were transfected with pCL (-Eco, or 10A1) packaging plasmids[54] plus pM6P.BLAST empty vector (kind gift of F. Randow, Cambridge, UK) or pM6P containing the cDNA of human or mouse iTAP or mouse iRhom2. WT or iTAP KO HEK 293ET cells were transduced with the viral supernatant supplemented with polybrene 8 µg/mL, and selected with blasticidin (8 µg/mL) to generate stable cell lines. To transduce RAW 264.7 or L929, lentiviruses were prepared and concentrated as follows: HEK 293FT cells (24 x 10^6) were transfected with pMD-VSVG envelope plasmid, psPAX2 helper plasmid and pLentiCas9-blast or empty vector pLentiGuide-puro or pLentiGuide-puro containing iTAP targeted gDNAs. The viral supernatants were concentrated 300-fold using ultracentrifugation (90,000 g) at 4°C for 4h, followed by re-suspension in 0.1 % BSA in PBS. Cells were transduced with the concentrated virus, supplemented with 8 µg/ml polybrene.

Generation of iTAP KO cells via CRISPR

For CRISPR-mediated knockout of iTAP in human cells, gRNAs targeting exons common to all transcripts: the 1st coding exon 5'-GCCCCGCTGAGCGATCCCAC-3' or coding exon 4 of *FRMD8* (iTAP) 5'-ACGTGTTCTTCCCAAAGCGG-3' were cloned into plentiCRISPR v2 (Addgene plasmid # 52961), a gift from Feng Zhang. For the ablation of iTAP in human cells, HEK 293ET cells (2.5 x 10^4 / cm^2) were transfected using Fugene with pLentiCRISPR v2 empty vector, or either of the pLentiCRISPR-derived sgRNA plasmids described above. The next day, the cells were selected with puromycin (8µg/mL) for 3 days until mock transfected cells were eliminated. Cells were expanded and single-cell sorted by FACS or serial dilutions on 10 cm culture plates. To screen for the presence of indels in clones, genomic DNA was extracted from each clone and a 200 bp region flanking the site targeted by the gRNA was amplified for exon 1 (forward = 5'-CCTCCAGCCCCCCATCCCTGGCTC-3'; reverse = 5'-GCCAGAGCTACTTCTCCAGGGCTGGGG-3') or exon 4 (forward = 5'-TCGGGAGAGGGGAGGGCTAAGCAG-3'; reverse = 5'-GGGCAAGGTGCGAATGTCCAGGGGTC-3'). Clones with mutant alleles were selected and the original PCR fragments amplified were isolated and sequenced via TOPO TA cloning. The selected clones "KO A" and "KO B" which contain indels in all alleles of *FRMD8*, were then confirmed for loss of iTAP at the protein level by immunoprecipitation and subsequent western blot with an anti-FRMD8 antibody. For the ablation of iTAP in HeLa cells, an

alternative approach was used: HeLas were transiently transfected with a pool of 3 gRNA plasmids (PX330, Zhang lab, Addgene 42230[55]) (TGACGTGCTGGTATACCTAG; GGAACGTGTTCTTCCCAAAG; GGCACTTGAGGAGATAGGCG) specifically targeting exons 2,4 and 6 of the human FRMD8 gene respectively, in conjunction with a plasmid encoding puromycin resistance (pEGFP-C1 from Clontech expressing a GFP-tagged puromycin N-acetyl-transferase). After puromycin selection, the efficient knockout of iTAP in the bulk population was confirmed by immunoblotting the lysates with iTAP antibodies, and by the significant depletion of mature TACE (Figure 6—figure supplement 1).

To ablate iTAP in mouse cells, gRNAs targeting the first coding exon (5'-TTCGGTGGGACCGCTCCGCA-3') or second coding exon (5'-GCACTACTGTATCATCCGCC-3') were cloned into plentiGuide-Puro (Addgene plasmid # 52963) and used in combination with lentiCas9-Blast (Addgene plasmid # 52962); both gifts of Feng Zhang. For transfection of the gRNAs, 2 x 10^5 L929 or 5 x 10^5 RAW 264.7 cells were transduced with 40 µl (RAW 264.7) or 20 µl (L929) of 300-fold concentrated lentivirus encoding pLentiCas9-Blast (Addgene #52962) and selected with blasticidin (4 µg/mL, RAW 264.7 and 8 µg/mL, L929). The Cas9-expressing lines were then transduced with the pLentiGuide-Puro sgRNA plasmds targeting the 1st or 2nd coding exons of mouse *Frmd8* (iTAP). Following selection with puromycin (4 µg/mL, RAW 264.7 and 7 µg/mL L929) the cells were single clone sorted by FACS. To screen for iTAP KO clones, genomic DNA was extracted from each clone and PCR used to amplify a 200bp region flanking the guide sequence (exon 1: forward= 5'TTGAGAGCTTGAGGAGACCA-3'; reverse 5'-CAGGCTGGAACCAAAGAGTTC-3'); exon 2: forward= 5'-GGAAATGCTGATTGGACCTC-3'; reverse 5'-CCTGCTGCCAGACCTTACCC-3'). Clones with mutant alleles were identified as described for human cells.

Experiments with mice

Experiments with mice were performed in accordance with protocols approved by the Ethics Committee of the Instituto Gulbenkian de Ciência and the Portuguese National Entity (DGAV-Direção Geral de Alimentação e Veterinária) and with the Portuguese (Decreto-Lei no. 113/2013) and European (directive 2010/63/EU) legislation related to housing, husbandry, and animal welfare.

Generation of iTAP mutant mice

iTAP mutant mice were generated via CRISPR/Cas9 as previously described[56,57]. In brief, two gRNA´s (5'-CAGCCGAGTGCAGATCGGGT-3' and 5'-GTGGCGGACTCAGAAATCAA-3') were designed to introduce a deletion of the first coding exon (exon 2) of the mouse *Frmd8* gene. Oligos encoding the gRNA were inserted into the plasmid pgRNAbasic[57], which contains a T7 promoter. The linearized vector was used as template for the production of sgRNAs, produced by *in vitro* transcription using the MEGAshortscript T7 Kit (Life Technologies). RNA was cleaned using the MEGAclear kit (AM1908, Life Technologies). Cas9 mRNA was produced by *in vitro* transcription using the mMESSAGE mMACHINE T7 Ultra Kit (Life Technologies) and plasmid

pT7-Cas9 as a template[57]. Cas9 mRNA (10 ng/ml), plus the sgRNAs (10 ng/ml) were injected into the pronuclei of fertilized C57 BL/6 oocytes using standard procedures[58]. Deletions were assessed by PCR from tail genomic DNA using primers 5′-CCCGACTTGTTTGGCCATTTC-3′ or 5'-CGGGGCCTCGGGTTTG-3' (forward) and 5′-TGGGACAAAGGAAGTGGTGCC-3′ (reverse). The deletion was confirmed by direct sequencing and TOPO-cloning followed by sequencing. These primers (along with 5'-ACTTTCACCCTACACATTTG-3' 5'-AGTCCGCCACATCTAAAC-3' for better amplification of WT alleles) were also used for genotyping mice and embryos of the iTAP KO line.

Immunostaining and fluorescence microscopy

HeLa (5 x 10^4 cells/well) were plated on coverslips and transfected with iTAP-GFP (600 ng) or iRhom2-Cherry (600 ng), either alone or in combination. After 24 h, cell supernatant was removed and cells were washed 3 times with PBS (2 mL). Cells were fixed with 3 % paraformaldehyde for 10 minutes. Cells were washed again 3 times with PBS (2 mL) followed by permeabilisation with 0.15 % TX100 for 15 minutes. Cells were blocked with 2 % BSA (in PBS, pH 7.2) for 1 h to reduce non-specific binding of antibodies. Specific primary antibodies against Calnexin (Cell Signaling, C5C9) and Golgi GM130 (BD, 610823) were diluted 1:100 in 2 % BSA. Primary antibodies were incubated for 2 h at room temperature. Cells were washed 3 times with PBS (2 mL). Cells were incubated with the relevant rhodamine red-conjugated secondary antibody (Alexa Fluor) diluted 1:1000 in 2 % BSA for 1 h at room temperature. Cells were washed again with PBS, followed by incubation with Hoechst (Sigma) for 10 minutes. Coverslips were mounted on slides with 5 □L of Slow Fade (Molecular Probes).

For mitotracker staining, cells were transfected with iTAP-GFP (600 ng), as described previously. After 24 h, cells were treated with Mitotracker-Red (50 nM) for 15 minutes at 37°C, followed by fixation with 3 % paraformaldehyde. Nuclei were stained with Hoechst. Cells were visualised and analysed using a laser scanning confocal microscope (Olympus FV1000) using a 488 nm Argon laser (green fluorescence), a 543 nm HeNe laser (red fluorescence) and a 405 nm LD laser. Confocal images were acquired using Fluroview 1000 V.1 software.

To investigate the lysosomal mis-sorting of mCherry-iRhom2 in iTAP deficient HeLa cells, 1µg mCherry-iRhom2 or 500ng mCherry-iRhom2 and 500ng iTAP-GFP were transfected into parental and iTAP KO HeLa cells using Fugene 6 (Promega). 48h post transfection, cells were fixed in 4% PFA in PBS, permeabilized with 0.2% Saponin in PBS, blocked in 0.1% Saponin/1% BSA in PBS and incubated with an antibody against the lysosomal marker LAMP2 and appropriate secondary antibodies. The cells expressing mCherry-iRhom2 and iTAP-GFP were also co-stained under the same conditions with the early endosome marker EEA1 to visualize a potential localization to endosomes.

Live fluorescence microscopy.

iRhom1/iRhom2 DKO MEFs expressing eGFP-miRhom2 alone or with mouse iTAP-mCherry (Figure 5H), or WT MEFs stably expressing eGFP-miRhom2, mTACE-GFP, mTACE-TagRFP, or

LAMP1-mCherry delivered by retroviral transduction (using pM6P derivatives) in the indicated combinations were plated (5 x 10^4 per well) on 4-chamber glass-bottomed dishes (In Vitro Scientific, D35C4-20-1.5-N) 24 hours prior to imaging, in the presence or absence of 10 µM Chloroquine as indicated. Cells were imaged on a laser scanning confocal microscope Zeiss LSM 780* using the 40x/1.2 M27 W Korr C-Apochromat objective and a 488nm or 561nm excitation wavelength.

***In vivo* protein cross-linking with Dithiobis Succinimidyl Proprionate (DSP)**

Cells are washed twice in cold PBS before incubation in 0.2 mg/mL DSP for 45min. The cross-linker was aspirated off and the cell monolayers were washed three times for 10 min in ice cold PBS containing 50 mM Tris, pH 8.0 to quench any remaining cross-linker. Subsequently the cells were lysed in Triton X-100 lysis buffer (150 mM NaCl, 50 mM Tris-HCl, protease inhibitors, pH 7.4 and 10 mM 1,10-phenanthroline). Post-nuclear supernatants were supplemented to contain 0.1% SDS and 0.25% sodium deoxycholate.

Co-immunoprecipitations

HEK 293ET cells expressing the indicated plasmids were lysed for 10 minutes on ice in TX-100 lysis buffer (1% Triton X-100, 150 mM NaCl, 50 mM Tris-HCl, pH 7.4) containing complete protease inhibitor cocktail (Roche), and 10 mM 1,10-phenanthroline (to inhibit TACE autoproteolysis) unless otherwise indicated. Post-nuclear supernatants were pre-cleared with unconjugated magnetic beads or agarose at 4°C for 60 minutes with rotation, followed by capture on anti-HA magnetic beads or anti-Flag respectively for 90 minutes. Beads were washed 3-5 times, for 10 minutes, at 4°C in the same Triton X-100 lysis buffer supplemented with NaCl to 300 mM. Samples were eluted with 1.5 x SDS-PAGE sample buffer and incubated at 65°C for 15 minutes before loading.

Identification of iRhom-interacting proteins

HEK 293ET cells were stably transduced with lentiviruses encoding pLEX empty vector, or pLEX derivatives containing HA-tagged iRhom1, iRhom2, iRhom1 N terminus, Rhbdd2, RHBDD3, Ubac2. Live cells were washed twice with ice-cold PBS, then left untreated or treated with the crosslinker DSP (0.2 mg/mL) as described below. Lysates were clarified, then pre-cleared with irrelevant control antibodies conjugated to magnetic beads for 60 min at 4°C with rotation. After saving 'input' samples, the lysates were incubated with anti-HA resin for 90 min at 4°C with rotation. Subsequently, the precipitated beads were washed four times in the respective buffers indicated above. One quarter of the beads were reserved for SDS-PAGE analysis, whereas three-quarters of the precipitated beads were resuspended in UREA buffer (8M Urea, 4% CHAPS, 100 mM DTT, 0.05% SDS). For MS analysis, immunoprecipitates were enzymatically digested on 3 kD MWCO filters (Pall Austria Filter GmbH) using an adaption of the FASP protocol as described previously[59,60]. After pre-concentration of the samples, protein reduction and alkylation was performed, then trypsin was added and incubated at 37°C for 18h. The digested peptide samples

were dried and stored at -20°C then later reconstituted in 5 µl 30% formic acid (FA) containing 10 fmol each of 4 synthetic standard peptides and further dilution with 40 µl mobile phase A (98% H_2O, 2% ACN, 0.1% FA), as described previously[59,61]. LC-MS/MS analyses were performed using a Dionex Ultimate 3000 nano LC-system coupled to a QExactive orbitrap mass spectrometer equipped with a nanospray ion source (Thermo Fisher Scientific). For LC-MS/MS analysis, 5 µl of the peptide solution were loaded and pre-concentrated on a 2 cm x75 µm C18 Pepmap100 pre-column (Thermo Fisher Scientific) at a flow rate of 10 µl/min using mobile phase A. Following this pre-concentration, peptides were eluted from the pre-column to a 50 cm x75 µm Pepmap100 analytical column (Thermo Fisher Scientific) at a flow rate of 300 nl/min and further separation was achieved using a gradient from 7% to 40% mobile phase B (80% ACN, 20% H_2O, 0.1% FA) over 85min including column washing and equilibration steps. For mass spectrometric analyses, MS scans were accomplished in the range from m/z 400-1400 at a resolution of 70000 (at m/z =200). Subsequently, data-dependent MS/MS scans of the 8 most abundant ions were performed using HCD fragmentation at 30% normalized collision energy and analyzed in the orbitrap at a resolution of 17500 (at m/z =200). Protein identification was achieved using Proteome Discoverer 1.4 (Thermo Fisher Scientific, Austria) running Mascot 2.5 (Matrix Science). Therefore, raw data were searched against the human proteome in the SwissProt Database (version 11/2015 with 20.193 entries) with a mass tolerance of 50 ppm at the MS1 level and 100 mmu at the MS2 level, allowing for up to two missed cleavages per peptide. Further search criteria included carbamidomethylation as fixed peptide modification and methionine oxidation as well as protein N-terminal acetylation as variable modifications.

Mass-spectrometry analysis of iTAP-interacting proteins

Lysates from HEK 293ET cells transfected with either empty vector, iTAP-FLAG, TNF-FLAG, STING-FLAG or SREBP2-FLAG and subjected to an immunoprecipitation with anti-FLAG M2 Affinity Gel. The beads were digested with mass spectrometry-grade porcine trypsin (Promega) 10ng/µl, in 2M urea, 50mM tris-HCL pH7.5 and 1mM DTT, overnight at 37°C. The peptides were alkylated with Iodoacetamide (Sigma), desalted using Empore™ Octadecyl C18 extraction disks and analysed on a Q-Exactive+ mass spectrometer coupled to a nano uHPLC (Thermo Fisher). Analysis was performed with MaxQuant 1.5.8.3 software. The abundance of the different interactors was determined with the average of protein peptides detected in each sample.

Cell surface biotinylation

Biotinylation was performed as previously described for BMDM with small modifications[15]. RAW 264.7 macrophages or iRhom2-HA HEK 293ET ($1.5x10^6$ cells, 6 well plates) were moved to a cold room (at 4°C), washed with ice-cold PBS pH 8.0 for 10 minutes, incubated with (1 mg/mL) Sulfo-NHS-LC-Biotin in PBS pH 8.0, according to the manufacturer's instructions. Following quenching with 50 mM Tris in PBS, cells were lysed for 10 minutes with TX-100 lysis buffer (1,10-phenathroline, protease inhibitors, 50 mM Tris), then biotin labelled surface proteins from post-nuclear supernatants were captured on neutravidin agarose resin at 4°C overnight. The resin was

washed 3 times, 10 minutes, with TX-100 lysis buffer containing 300 mM NaCl at 4°C. Samples were eluted with 1.5x SDS-PAGE sample buffer and incubated at 65°C for 15 minutes, before loading.

Glycoprotein enrichment using Concanavalin A

To improve the detection of TACE, cells were lysed in TX-100 lysis buffer supplemented with 1 mM EDTA, 1 mM $MnCl_2$, 1 mM $CaCl_2$ and glycoproteins were captured using Concanavalin A (ConA) Agarose. Beads were washed twice in the same buffer and eluted by heating for 15 min at 65°C in sample buffer supplemented with 15% sucrose or for 5 min at 95°C in sample buffer supplemented with 15% sucrose and 1x Glycoprotein denaturation buffer (NEB).

***In vitro* protein deglycosylation analysis**

Post-nuclear lysate supernatants or denatured lysates, are denatured at 65°C for 15min in the presence of 1x Glycoprotein Denaturing buffer (NEB). Endo-H and PNGase F reactions are set up according to manufacturer's instructions for 1h at 37°C.

Shedding and secretion assays

Shedding assays were performed using previously described plasmids encoding alkaline phosphatase-tagged EGFR ligands: Transforming Growth Factor α (TGFα), Amphiregulin (AREG), Epiregulin (EPIREG), Heparin Binding-Epidermal Growth Factor (HB-EGF), Epidermal Growth Factor (EGF) and Betacellulin (BTC) or Tumor necrosis factor (TNF)[62,63]. HEK 293ET (3 x 105 in 6 well-plates) were transfected with 1 µg cDNA of AP-substrates and 6 µL PEI. 48h later, cells were washed 3 times with serum free media before incubation for 1 hour in 1 mL Optimem (containing the vehicle of the drug in next step) (for basal shedding), followed by 1 hour with 1 mL Optimem containing 1 µM PMA (Phorbol 12-myristate 13-acetate) or 2.5 µM IO (Ionomycin; for stimulated shedding). Supernatants from each incubation step were collected. Following, the cells were washed in ice-cold PBS three times and lysed in Triton X-100 buffer described previously (unshed material). Supernatants and lysates were centrifuged on a bench-top centrifuge at top speed for 10 min to remove cells and cell debris. Supernatants and lysates were incubated with the Alkaline Phosphate (AP) substrate p-nitrophenyl phosphate (pNPP) at room temperature. AP activity measured using a 96-well plate spectrophotometer (405 nm). Results are presented as PMA or IO "shedding over total" calculated by the formula ('cleared stimulated shedding') / ('cleared stimulated shedding' plus 'unshed'). 'Cleared stimulated shedding' denotes 'stimulated shedding' minus 'basal shedding'. The release into the medium of a secreted form of luciferase containing a signal peptide was assessed as a control, as described[18].

***In vitro* TACE enzymatic activity assay.**

The assay was performed as previously described[15]. In brief, 8 million HEK 293ET cells were lysed for 10 minutes on ice in 1% Triton X-100, 150 mM NaCl, 50 mM Tris-HCl, pH 7.4 containing complete protease inhibitors cocktail (Roche). Importantly, all steps were performed in the

absence of the metalloprotease inhibitor 1,10-phenanthroline to preserve TACE activity. As previously described[14] when lysates are made in the absence of 1,10-Phenathroline, TACE autocatalytically cleaves off its cytoplasmic tail, result in loss of the epitope detected by the rabbit polyclonal antibody (Ab39162, Abcam) used for western blotting[15]. Therefore, mouse anti-TACE (9301, R&D), which recognizes an epitope within the ectodomain, was used for immunoprecipitations, to ensure that TACE was captured regardless of autocatalysis. Mature TACE without its cytoplasmic domain retains proteolytic activity *in vitro*[15]. Anti-TACE or mouse IgG (anti-GFP; mock) antibodies were incubated overnight with lysates, followed by capture of the immunocomplexes with anti-mouse magnetic beads. Immunoprecipitates were mixed with the fluorogenic TACE substrate peptide (ENZO Life Sciences, BML-P235-0001) and fluorescence was measured over 3 hours on a Victor 3 plate reader at 37°C, according to manufacturer instructions. As the western blots used the rabbit polyclonal antibody (Ab39162, Abcam), immunoprecipitates consequently show no evidence of mature TACE.

Protein extraction from mouse tissues

Protein was extracted from mouse tissues by lysing in a modified RIPA buffer (150 mM NaCl, 50 mM Tris-HCl, pH 7.4, 1 mM EDTA, 1% Triton X-100, 1% Na Deoxycholic Acid, 0.1% SDS containing protease inhibitors and 10 mM 1,10-phenanthroline). Homogenates were clarified and normalized, then incubated with ConA resin, as described above.

Densitometry

Semi-quantitative densitometric analysis on scanned images from western blot exposures was performed with Fiji software, measuring at least 3 independent experiments. Results represent mean values ± standard deviation. Half-life was calculated using GraphPad Prism software.

Alignments

Alignments were performed using Geneious software using the CLUSTALW algorithm.

Statistical analysis

All statistical analyses were done with two-sample two tail unpaired t-tests assuming unequal variances, using excel software. In Figure 3, comparisons were performed after transforming the raw values into their relative (fold change) values to the WT sample. The Pearson's correlation and Mander's colocalization coefficient were calculated after appropriate thresholding with the Volocity (Perkin Elmer) image analysis package. Thresholds were applied evenly across conditions. For the statistical analysis of the Pearson's correlation, the Pearson's taken from at least 20 individual cells acquired over two independent experiments were subjected to unpaired, two tailed t-tests in Excel. P-Values above 0.05 were considered as not significant.

Table 1. iTAP interacts with endogenous iRhoms. Lysates from HEK 293ET cells expressing iTAP-FLAG versus cells containing empty vector or expressing a panel of control proteins (TNF-FLAG, STING-FLAG, SREBP2-FLAG) were immunoprecipitated for FLAG and subjected to mass spectrometry. Peptides assigned to iRhom-1 or iRhom2 are found specifically in iTAP precipitates.

iRhom1	**Vector**	**iTAP**	**TNF**	**STING**	**SREBP2**
Peptide counts	0	**27**	0	0	0
Sequence coverage [%]	0	**37.7**	0	0	0

iRhom2	**Vector**	**iTAP**	**TNF**	**STING**	**SREBP2**
Peptide counts	3	**44**	2	2	2
Sequence coverage [%]	2.9	**45.4**	1.8	2.2	2

Table 2. Mendelian ratios of embryos isolated at embryonic day 14.5 (E14.5), or pups at (P1) post-partum obtained from crosses obtained between iTAP heterozygous mice.

Developmental Stage	iTAP +/+	iTAP +/-	iTAP -/-	Total No. of Animals
E14.5	10	17	4	31
%	32.2	54.8	12.9	
Ratio	1	1,7	0,4	
P1	54	116	50	220
%	24.55	52.73	22.73	
Ratio	1	2.14	0.93	

Acknowledgements

We thank Duarte Barral, Felix Randow, Shigeki Higashiyama, Jürgen Scheller and Feng Zhang for plasmids and Joachim Grötzinger for anti-TACE antibodies. We thank Matthew Freeman for helpful discussions. We thanks Duarte Barral, Maria João Amorim and Claudia Almeida helpful discussions. We express our gratitude to Moises Mallo for advice concerning CRISPR, CRISPR reagents and the generation of iTAP KO mice. We are grateful for the assistance of Ana Nóvoa and IGC's transgenics and mouse facilities. We thank the Life Imaging Center (LIC) of the University of Freiburg for their support regarding the analysis of iRhom2 and lysosomes. We thank IGC's cell sorting/flow cytometry, sequencing, and histopathology facilities and IGC's antibody service (Ana Regalado). We thank Petra Rampírová for cloning and technical assistance. CA acknowledges the support of Fundação Calouste Gulbenkian, Worldwide Cancer Research (14-1289), a Marie Curie Career Integration Grant (project no. 618769), Fundação para a Ciência e Tecnologica (FCT, SFRH/BCC/52507/2014; PTDC/BEX-BCM/3015/2014; LISBOA-01-0145-FEDER-031330) the European Crohn's and Colitis organization (ECCO), and COST BM1406. SJM acknowledges the support of Science Foundation Ireland (14/IA/2622). KS acknowledges the support of EMBO (Installation Grant no. 2329), Ministry of Education, Youth and Sports of the Czech Republic (project no. LO1302) and European Regional Development Fund (project OPPK no. CZ.2.16/3.1.00/24016). F.S was supported by an Emmy Noether scholarship from the German Research Council, DFG STE2310/1-1. IO acknowledges the support of Fundação Calouste Gulbenkian – IGC (fellowship contract as ref. 91/BD/14). M.C. acknowledges the support of the FCT (grant SFRH/ BPD/117216/2016). This work was developed with the support of the research infrastructure Congento, project LISBOA-01-0145-FEDER-022170, co-financed by Lisboa Regional Operational Programme (Lisboa 2020), under the Portugal 2020 Partnership Agreement, through the European Regional Development Fund (ERDF), and Foundation for Science and Technology (Portugal).

Conflicts of interest

The authors declare no conflicts of interest.

Figures, figure—supplements and source data

Figure 1. Identification of iTAP as a novel iRhom-interacting protein. (**A**). Schematic diagram showing the stable HEK 293ET cell lines expressing iRhom proteins or related rhomboid pseudoproteases as controls, which were subjected to immunoprecipitation followed by mass spectrometry. (**B**). An example immunoprecipitation indicating that only immunoprecipitates from cell lines expressing WT iRhom1 or iRhom2 contain the binding of the positive control protein, TACE. Here and throughout, immature and mature species of TACE are indicated with white and black arrows respectively. The red arrowheads show the full-length forms of the individual rhomboid-like proteins. (**C**). Peptides identified by mass spec that were assigned to FRMD8/iTAP. These peptides were found in immunoprecipitates from iRhom1, iRhom2 or the N-terminus of iRhom1 but not in the other samples. The peptides are shown from a representative experiment. All of the peptides found in the iRhom immunoprecipitates were mapped onto the human FRMD8 amino acid sequence (indicated in red). (**D**). Schematic diagram illustrating the domain structure of human FRMD8/iTAP. Beneath is shown a CLUSTALW alignment of the pfam FERM-M consensus (pfam00373) alongside FRMD8/iTAP. Identical residues are annotated in black and similar residues in grey.

Figure 1—figure supplement 1. iTAP is broadly expressed in a variety of tissues important for TACE biology. (**A**). Lysates were prepared from a panel of tissues from WT C57 BL/6J mice and iTAP was detected by western blot. Lysates from WT versus iTAP KO L929 mouse fibroblasts were used as a control. (**B**). The extent of co-expression between iTAP/Frmd8, TACE/ADAM17, iRhom2 or iRhom1 in mouse anatomical parts and cell types was investigated by interrogating gene expression data from the GeneChip™ Mouse Genome 430 2.0 Array via the Genevestigator platform[64].

Figure 2. Validation of iTAP binding to iRhoms. (**A**). iTAP binds specifically to iRhom -1 and -2. Human iTAP-FLAG was transfected into HEK 293ET cells alongside empty vector or the indicated HA-tagged iRhoms, their deletion mutants or the rhomboid pseudoproteases Ubac2 or Rhbdd2. HA proteins were immunoprecipitated and FLAG binding was assessed by western blot. (**B**). Schematic diagram indicating truncation mutants of the iRhom2 cytoplasmic tail that were generated to map the iTAP binding region. The cytoplasmic tail of iRhom2 was divided into 6 arbitrary portions. (**C,D**). iTAP binds to iRhom2 within an area defined by region 4 of iRhom2 (192-271aa). HEK 293ET cells were transfected with iTAP-FLAG and iRhom2-HA full length (FL) or the indicated iRhom2-HA deletion constructs shown in (B). Anti-HA immunoprecipitates were assessed for the binding of iTAP-FLAG by western blotting.

Figure 2—figure supplement 1. Cellular localization of iTAP. (**A**). HeLa cells were transfected with iTAP-GFP. After 24 h, cells were fixed, permeabilised and immunostained, as indicated, with specific antibodies against Golgi (GM-130) or ER (Calnexin) markers. The fluorescent dye Mitotracker-Red was used to visualise mitochondria. DNA was stained with Hoechst (blue). (**B**). HeLa cells were transfected with iTAP-GFP alone, or in the presence of iRhom2-Cherry, as indicated. After 24 h, cells

were fixed and stained with Hoechst to visualise DNA (blue). Images were acquired by confocal microscopy.

Figure 3. KO of iTAP diminishes TACE proteolytic activity. (**A**). Anti-iTAP immunoprecipitates from WT versus iTAP KO HEK 293ET cells were analyzed by immunoblotting. A GAPDH blot is the loading control for the inputs. Non-specific bands are indicated by white asterisks. (**B**)**.** PMA-stimulated TACE shedding is impaired in iTAP KO cells. The TACE substrates [Amphiregulin (AREG), Epiregulin (EPIREG), Heparin Binding-Epidermal Growth Factor (HB-EGF), Transforming Growth Factor-α (TGFα) and Tumor Necrosis Factor (TNF)] fused to alkaline phosphatase (AP) were transfected into HEK 293ET WT or iTAP KO cells. TACE activity was assessed based on AP activity secreted into the supernatant of the cells as described in materials and methods. (**C,D**). Expression of iTAP rescues the impaired shedding in iTAP KO cells. WT or iTAP KO HEK 293ET cells stably expressing empty vector or human iTAP were transfected with AREG-AP or TGFα-AP, then challenged in PMA shedding assays as described above. (**E**). The shedding impairment is specific to TACE. ADAM10 AP-fused substrates [Betacellulin (BTC) and Epidermal Growth Factor (EGF)] were transfected into the WT vs iTAP KO HEK 293ET cells. The cells were treated with the ADAM10 stimulant Ionomycin (IO) and AP activity was measured in the medium. (**F**). Global secretion is not impaired in iTAP KO cells. WT or iTAP KO cells were transfected with secreted luciferase and luciferase associated luminescence was measured in the supernatant of PMA-stimulated cells (upper graph) or vehicle (DMSO, lower graph). Here and throughout: KO 'A' and KO 'B' denotes independent iTAP KO HEK 293ET clones. PMA (1 μM) or IO (2.5 μM) incubations took place for 1h following serum starvation. Shedding or secretion values are expressed as fold change relative to WT cells. Data are presented as mean ± standard deviation and represent at least 3 independent experiments. * = p≤0.05, ** = p≤0.01, *** = p≤0.001 and n.s. = non-significant.

Figure 3—figure supplement 1. Assessment of proteolytic activity in TACE IPs from WT versus iTAP KO cells. TACE immunoprecipitates (IPs) were used in a TACE substrate cleavage assay. (**A**). The specificity of the TACE antibody in immunoprecipitations is demonstrated by probing IPs with TACE and transferrin Receptor (TfR) antibodies. To avoid blocking TACE activity, the IPs and subsequent assays were performed in the absence of 1,10-phenathroline (phen.). As post-lysis TACE cleaves off the cytoplasmic tail containing the epitope recognized by the western blotting antibody, only the immature form of TACE is detected by immunoblotting (see Materials and methods for details). A ConA enriched lysate, prepared in the presence of 1,10-phenathroline, is shown on the left-hand side as a positive control for TACE detection. (**B**). Total TACE immunoprecipitates from WT or iTAP KO HEK 293ET cells were subjected to a TACE peptide-substrate fluorogenic cleavage assay. Data are presented as mean ± standard error of 3 independent experiments. ** = p≤0.01.

Figure 3—source data 1: PMA-stimulated TACE shedding is impaired in iTAP KO cells. Alkaline phosphatase assays with TACE substrates.

Figure 3—source data 2: Expression of iTAP rescues the impaired shedding in iTAP KO cells. Alkaline phosphatase assays with TACE substrates -/+ iTAP.

Figure 3—source data 3: The shedding impairment is specific to TACE. Alkaline phosphatase assays with ADAM10 substrates.

Figure 3—source data 4: Global secretion is not impaired in iTAP KO cells. Secreted luciferase.

Figure 3—figure supplement 1—source data 1: iTAP ablation impairs the performance of TACE in activity assays.

Figure 4. Mature TACE is specifically depleted in iTAP KO cells. (**A**). iTAP was knocked out in L929, RAW 264.7 and HEK 293ET cells using CRISPR. Lysates were immunoblotted with anti-iTAP antibodies. A small black arrowhead indicates iTAP protein whereas a non-specific band (white asterisk) serves as a loading control. (**B**). Glycoproteins from lysates isolated from the cells in (A) were enriched using concanavalin A-sepharose (conA) and TACE levels were assessed by western blot. Here and throughout, the immature form of TACE is indicated by a white arrow, whereas, the mature form is denoted by a black arrow. iRhom double KO MEFs were used as a reference and the transferrin receptor (TfR) as a loading control. Lower panels: densitometry in HEK 293ET. Left hand panel: Levels of immature TACE normalized to TfR. Right hand panel: levels of mature TACE as a relative proportion of immature TACE in WT and iTAP KO HEK 293ET. (**C,D**). Validation of mature and immature TACE detection in panels of WT versus iRhom2 DKO (C) or iTAP KO (D) cells, by deglycosylation. ConA enriched lysates from the cell lines in (A) were treated with endoglycosidase H (Endo-H; H; which cleaves ER-resident glycans only) and PNGase F (F; which cleaves both ER and post-ER glycans). Here and throughout: the immature TACE is indicated with white arrowheads; the black arrowhead denotes both glycosylated mature TACE and deglycosylated immature TACE respectively (which have similar electrophoretic mobility), whereas red arrowheads denote the fully deglycosylated, mature, TACE polypeptide. (**E**). iTAP expression restores the presence of mature TACE in iTAP KO cells. Lysates from WT or iTAP KO HEK 293ET stably expressing empty vector (-, EV) or human iTAP (+) were screened for mature TACE. Actin was used as a loading control. Middle and lower panels: densitometric analysis indicates that iTAP expression increases the levels of mature TACE but does not affect the levels of immature TACE. Middle panel: levels of mature TACE as a relative proportion of immature TACE in WT and KO upon iTAP or EV expression in WT and iTAP KO HEK 293ET clones. Lower panel: Levels of immature TACE after normalization to actin. (**F**). iTAP KO cells lack mature cell surface TACE. Left hand panel: RAW 264.7 WT or iTAP KO were surface-biotinylated *in vivo* and lysates were enriched for biotinylated proteins with neutravidin resin. Probing for TfR was used as a cell surface positive control protein whereas anti-p97 probing demonstrates that intracellular proteins were not labeled. Right hand panel: Cell surface biotinylated proteins were deglycosylated using Endo-H (H) or PNGase F (F). ConA enriched lysates were run as mobility controls, for immature and mature TACE. Blots were probed for TACE and for TfR as a control protein. (**G**). Loss of iTAP has no impact on the mature species of other ADAM metalloproteases. HEK 293ET WT or KO cells were transfected with the indicated panel of V5-tagged ADAMs. The lysates were deglycosylated as described above and Tubulin serves as a loading control. Throughout: Data are presented as mean ± standard deviation and represent 3 independent experiments. * = $p \leq 0.05$, ** = $p \leq 0.01$, *** = $p \leq 0.001$ and n.s. = non-significant.

Figure 4—source data 1: iTAP KO cells are depleted in mature TACE levels. Densitometric analyses of mature/immature TACE levels.

Figure 4—source data 2: iTAP expression restores the presence of mature TACE in iTAP KO cells. Densitometric analyses of mature/immature TACE levels.

Figure 5. iTAP is required to promote iRhom stability at the cell surface. (**A**). iRhom2 is depleted in iTAP KO cells. Lysates from WT vs iTAP KO RAW 264.7 were probed for endogenous iRhom2. The transferrin receptor (TfR) is a loading control. (**B**). iTAP expression enhances the stability of iRhom2. Stable iRhom2-HA-expressing HEK 293ET were transiently transfected with empty vector (EV) or iTAP-FLAG. 48h post-transfection, the cells were treated with 100 µg/mL Cycloheximide (CHX) for the indicated durations. The stability of iRhom2 was assessed by HA blotting. The graph to the right of the panel indicates the relative density of iRhom2-HA bands from cells expressing EV (black) versus iTAP (red). The half-life of iRhom2 under both conditions is calculated. (**C**). iTAP and iRhom2 co-localize. HeLa cells were transfected with iTAP-GFP and mCherry-iRhom2. Two areas, A and B, were selected for the calculation of the Pearson's correlation and Manders' colocalization co-efficients, respectively. (**D**). iTAP expression enhances the post-ER form of iRhom2. HEK 293ET expressing stably iRhom2-HA minus or plus stably expressed iTAP-FLAG were deglycosylated with Endo-H or PNGAse F. (**E**). iRhom2-HA stably expressing HEK 293ET cells were transiently transfected with EV or iTAP-FLAG. Cells were treated -/+ the thiol-reducible cell-permeable crosslinker, DSP, and then anti-FLAG immunoprecipitations were performed from the lysates. Prior to SDS-PAGE and immunoblotting, lysates and co-immunoprecipitates were denatured in the presence of DTT to break the DSP-mediated covalent cross-links. Samples containing iRhom2-HA were deglycosylated as described before. (**F**). ER exit of iRhom2 is not impaired in iTAP KO cells. WT or iTAP KO HEK 293ET were transiently transfected with iRhom2-HA. Their lysates were deglycosylated as described. Endo-H–sensitive (black arrowhead) and –insensitive (white arrowhead) bands are noted. (**G**). iTAP expression stabilizes iRhom2 on the cell surface. The same cell lines as in (B), (E), were subject to a cell surface biotinylation protocol and the cell surface levels of iRhom2 in response to CHX treatment were evaluated. The graphs on the right hand side show densitometric analysis of the surface fractions of iRhom2-HA (upper graph) or TfR (lower graph) (**H**). iRhom1/2 DKO MEFs stably expressing eGFP-mouse iRhom2 either alone or together with mouse iTAP-mCherry were imaged as live cells. The GFP-iRhom2 signal is shown.

Figure 5—figure supplement 1. iTAP ablation increases iRhom2 degradation but doesn't affect its ER exit. (A). Absence of iTAP destabilizes iRhom2. WT or iTAP KO HEK 293ET cells were transiently transfected with iRhom2-HA. 48h post transfection, the cells were treated with 100 µg/mL CHX for the indicated durations. The stability of iRhom2 was then assessed by HA blotting. Tubulin was used as loading control. (**B**). Deglycosylation of endogenous iRhom2 in lysates from WT versus iTAP KO RAW 264.7 cells. The lysates were run on 4-12% gradient gels. The arrowheads in the Endo-H lanes denote a doublet containing Endo-H sensitive (upper arrowhead) and insensitive (lower

arrowhead) species of iRhom2 detected in both WT and iTAP KO cells. The two panels at the bottom are cropped from the upper (WT) versus 3rd from top (KO) iRhom2 exposures respectively. The two, cropped images were grouped together, then artificially stretched, to the same degree, along the Y axis to accentuate the difference in iRhom2 mobility in response to Endo-H versus PNGase F.

Figure 5—source data 1: iTAP expression enhances the stability and half-life of iRhom2. Densitometric analysis on iRhom2-HA in a CHX course.

Figure 5—source data 2: iTAP expression stabilizes iRhom2 on the cell surface. Densitometric analysis of the cell surface fractions of iRhom2-HA or TfR.

Figure 6. iTAP is required to prevent the trafficking of the sheddase complex to the lysosomes, where iRhom2/TACE are degraded. (**A**)**.** WT or iTAP KO HeLa cells were co-transfected with mCherry-iRhom2. Fixed cells were immunostained for the lysosomal marker LAMP2 and stained with DAPI. iRhom2/LAMP2 co-localization was quantified (right-hand graph). (**B**). The phenotype observed in (A) is reverted upon the co-expression of iTAP-GFP, resulting in no co-localization of mCherry-iRhom2 with endogenous LAMP2. (**C**). WT or iTAP KO RAW 264.7 cells were treated with 50 µM Chloroquine (CQ) for 48h, 100 µM Bafilomycin (Baf) for 16h, or 10 mM ammonium chloride (NH_4Cl) for 48h and endogenous iRhom2 levels were detected by western blotting. Actin or tubulin were used as loading controls and the Transferrin Receptor (TfR) acts as a control for the inhibition of lysosomal hydrolases. (**D**). Lysates from cells treated with Baf as described above, were conA-enriched and probed for TACE on a western blot. Tubulin and TfR are controls for loading and lysosomal inhibition, respectively. (**E**) In the left-hand panel, eGFP-iRhom2 was stably expressed in WT MEFs (expressing endogenous iTAP) in the presence of lysosomal marker LAMP1-mCherry, and the subcellular localization of both proteins was imaged in live cells using confocal microscopy in the absence (upper row) or presence (lower row) of 10 µM Chloroquine. The results indicate that iRhom2 alone is trafficked into the lysosomes. In the right-hand panel, WT MEFs stably expressing TACE-eGFP and LAMP1-mCherry in the presence of 10 µM Chloroquine were imaged similarly. The results indicate that TACE alone does not localize in lysosomes (upper row). However, lysosomal trafficking of TACE-TagRFP is induced by the presence of co-expressed eGFP-miRhom2 (lower row).

Figure 6—figure supplement 1. Validation of iTAP KO in HeLa cells. Lysates (3 technical replicates) from WT vs iTAP KO HeLa cells were immunoblotted with antibodies specific to iTAP (upper panel) or WASHC5 as a loading control.

Figure 6—source data 1: Quantification of mCherry-iRhom2 /LAMP2 colocalization analyses.

Figure 7. iTAP is essential for TACE maturation and function in primary cells and tissues from human and mouse. (**A**). Schematic representation of the CRISPR targeting strategy to delete mouse *Frmd8* (iTAP) gene using two guide RNAs flanking the first coding exon (exon 2). In the upper

schematic of the *Frmd8* locus, open boxes indicate non-coding exons whereas filled boxes indicate coding exons (**B**). Mouse embryonic fibroblasts (MEFs) were isolated from WT versus two independent iTAP KO E14.5 embryo littermates. The loss of iTAP at the protein level is shown by immunoblotting. (**C**). Mature TACE is diminished in iTAP KO MEFs. ConA-enriched lysates from MEFs isolated from WT versus iTAP KO embryos were deglycosylated as described previously. The transferrin receptor (TfR) is used as a loading control. (**D**). Mature TACE is depleted or diminished in TACE-relevant tissues from iTAP KO mice. ConA-enriched lysates from WT vs iTAP KO mouse tissues and bone marrow-derived macrophages, were deglycosylated as described previously. TACE was detected by western blot. The immature and mature species of TACE are indicated with white arrowheads and black arrowheads respectively, whereas red arrowheads denote the fully deglycosylated mature polypeptide. The experiment was performed twice with lysates isolated from tissues from two individual KO mice. (**E**). iTAP is essential for TACE physiological regulation in human primary cells. Isolated primary human peripheral blood mononuclear cells (PBMC) were differentiated into monocytes, then electroporated with the indicated siRNAs. Cells were then stimulated with the indicated concentrations of lipopolysaccharide (LPS). After 18h, the concentration of the cytokines TNF, IL-6 and IL-8 secreted into the supernatants, was measured by ELISA. The experiment was done three independent times and data from one representative experiment is shown. Data presented as mean ± standard error from triplicate measurements.

Figure 7—figure supplement 1. Mouse *Frmd8*/iTAP gene targeting via CRISPR. (**A**). Schematic diagram showing the *Frmd8* locus. Non-coding exons are denoted by open rectangles, whereas coding exons are shaded black. An enlarged area showing *Frmd8* exons 1 and 2 is included to indicate the regions targeted by the CRISPR strategy. (**B**,**C**). Detailed maps of the WT and mutant loci of two different *Frmd8* KO founder lines that were generated. A pair of gRNAs (indicated in red) was selected to engineer the deletion of the first coding exon of mouse *Frmd8* as described in materials and methods. The PAM sequence and the theoretical Cas9 cut sites 3-4 bp from the PAM are indicated. The resulting founder animals were genotyped from tail biopsies and the identity of the lesions revealed by DNA sequencing. Two lines of animals (1 and 2) were established following germline transmission of the mutant alleles from individual founders. (**B**). KO line **1** contains a 478 bp deletion that removes exon 2 along with parts of introns 1 and 2. (**C**). KO line **2** contains a larger deletion of 625 bp that starts within the non-coding exon 1, deletes all of intron 1, exon 2 and part of intron 2, as shown. In both cases, the precise nucleotide sequence on the 5' and 3' boundaries of the mutant lines is indicated and aligned with the WT genomic sequence. The loss of iTAP at the protein level in both founder lines was confirmed by western blotting.

Figure 7—source data 1: iTAP is essential for TNF secretion in primary macrophages. TNF ELISA.

Figure 7—source data 2: iTAP is not essential for IL-6 secretion. IL-6 ELISA.

Figure 7—source data 3: iTAP is not essential for IL-8 secretion. IL-8 ELISA.

Figure 8. Schematic model showing regulation of the cell surface stability of the sheddase complex by iTAP. (**A**). In WT cells the iRhom2/TACE sheddase complex successfully transits from the ER to the Golgi apparatus, where TACE undergoes maturation (prodomain removal). The sheddase complex then traffics to the cell surface, where TACE cleaves it substrates (e.g. TNF, EGFR ligands), enabling their release for signaling. iTAP, which loads onto the sheddase complex in the ER, remains associated with the sheddase complex and ensures the stability of the complex on the cell surface, promoting the cleavage of TACE substrates. (**B**). By contrast, in iTAP KO cells, the sheddase complex is aberrantly sorted to the lysosome, where iRhom2 and mature TACE are degraded. As a result, no TACE substrates are released for signaling. The dotted arrows indicate a putative itinerary taken by the sheddase complex in iTAP KO cells. The sheddase complex may be destabilized on the cell surface: aberrantly targeted for endocytosis and shunted to the lysosome. Alternatively, the sheddase complex may be endocytosed from the cell surface at the normal rate, but loss of iTAP may result in a defect in recycling the complex back to the cell surface, favouring delivery to the lysosome.

Figure 8—figure supplement 1. iTAP does not bind to features commonly recognized by FERM domain proteins. (**A**). iTAP appears not to have a high affinity for actin. HEK 293ET cells transiently expressing vector or iRhom2-HA and iTAP-FLAG were starved overnight then stimulated with or without PMA (1µM) for 30min. PMA was shown to alter the steady state of iRhom interactions with clients[25] and hence is used to assess potentially differential binding upon stimulated conditions. An anti-FLAG IP was performed on the cell lysates and binding was assessed by western blotting (**B**). Schematic representation of the location of the NxxY motifs within the iRhom2 sequence. NxxY is a common consensus binding motif for FERM proteins (eg sorting nexins) that participate in vesicular sorting functions. (**C**). iTAP binding is independent of NxxY motifs. HEK 293ET cells were transiently transfected with iTAP-FLAG and vector, iRhom2-HA, single (left hand panel) or double (right hand panel) NxxY>AAAA mutants of iRhom2-HA, or Ubac2-HA as a negative control. Cell lysates were subjected to anti-HA co-precipitation. iTAP binding to iRhom was assessed by western blotting. (**D**). iTAP does not co-localize with early endosomes. HeLa cells co-expressing iTAP-GFP and mCherry-iRhom2 were immunostained for EEA1, a marker of early endosomes. The white box indicates a magnified area that is separated into all three channels in the right hand images.

Table legends

Table 1. iTAP interacts with endogenous iRhoms. Lysates from HEK 293ET cells expressing iTAP-FLAG versus cells containing empty vector or expressing a panel of control proteins (TNF-FLAG, STING-FLAG, SREBP2-FLAG) were immunoprecipitated for FLAG and subjected to mass spectrometry. Peptides assigned to iRhom-1 or iRhom2 are found specifically in iTAP precipitates.

Table 2. Mendelian ratios of embryos isolated at embryonic day 14.5 (E14.5), or pups at (P1) post-partum obtained from crosses obtained between *Frmd8* (iTAP) heterozygous mice.

References

1. Brenner, D., Blaser, H. & Mak, T. W. Regulation of tumour necrosis factor signalling: live or let die. *Nat Rev Immunol* **15**, 362-374 (2015).
2. Locksley, R. M., Killeen, N. & Lenardo, M. J. The TNF and TNF receptor superfamilies-integrating mammalian biology. *Cell* **104**, 487-501 (2001).
3. Kleijwegt, F. S. et al. Critical role for TNF in the induction of human antigen-specific regulatory T cells by tolerogenic dendritic cells. *J Immunol* **185**, 1412-1418 (2010).
4. Richter, C. et al. The tumor necrosis factor receptor stalk regions define responsiveness to soluble versus membrane-bound ligand. *Mol Cell Biol* **32**, 2515-2529 (2012).
5. Grell, M. et al. The transmembrane form of tumor necrosis factor is the prime activating ligand of the 80 kDa tumor necrosis factor receptor. *Cell* **83**, 793-802 (1995).
6. Ruuls, S. R. et al. Membrane-bound TNF supports secondary lymphoid organ structure but is subservient to secreted TNF in driving autoimmune inflammation. *Immunity* **15**, 533-543 (2001).
7. Alexopoulou, L. et al. Transmembrane TNF protects mutant mice against intracellular bacterial infections, chronic inflammation and autoimmunity. *Eur J Immunol* **36**, 2768-2780 (2006).
8. Horiuchi, K. et al. Cutting edge: TNF-alpha-converting enzyme (TACE/ADAM17) inactivation in mouse myeloid cells prevents lethality from endotoxin shock. *J Immunol* **179**, 2686-2689 (2007).
9. Peschon, J. J. et al. An essential role for ectodomain shedding in mammalian development. *Science* **282**, 1281-1284 (1998).
10. Gooz, M. ADAM-17: the enzyme that does it all. *Crit Rev Biochem Mol Biol* **45**, 146-169 (2010).
11. Zunke, F. & Rose-John, S. The shedding protease ADAM17: Physiology and pathophysiology. *Biochim Biophys Acta* **1864**, 2059-2070 (2017).
12. Murphy, G. Regulation of the proteolytic disintegrin metalloproteinases, the 'Sheddases'. *Semin Cell Dev Biol* **20**, 138-145 (2009).
13. Grötzinger, J., Lorenzen, I. & Düsterhöft, S. Molecular insights into the multilayered regulation of ADAM17: The role of the extracellular region. *Biochim Biophys Acta* **1864**, 2088-2095 (2017).
14. Schlondorff, J., Becherer, J. D. & Blobel, C. P. Intracellular maturation and localization of the tumour necrosis factor alpha convertase (TACE). *Biochem J* **347 Pt 1**, 131-138 (2000).
15. Adrain, C., Zettl, M., Christova, Y., Taylor, N. & Freeman, M. Tumor Necrosis Factor Signaling Requires iRhom2 to Promote Trafficking and Activation of TACE. *Science* **335**, 225-228 (2012).
16. McIlwain, D. R. et al. iRhom2 Regulation of TACE Controls TNF-Mediated Protection Against Listeria and Responses to LPS. *Science* **335**, 229-232 (2012).
17. Li, X. et al. iRhoms 1 and 2 are essential upstream regulators of ADAM17-dependent EGFR signaling. *Proc Natl Acad Sci U S A* **112**, 6080-6085 (2015).
18. Christova, Y., Adrain, C., Bambrough, P., Ibrahim, A. & Freeman, M. Mammalian iRhoms have distinct physiological functions including an essential role in TACE regulation. *EMBO Rep* **14**, 884-890 (2013).
19. Siggs, O. M. et al. iRhom2 is required for the secretion of mouse TNFalpha. *Blood* **119**, 5769-5771 (2012).
20. Arribas, J. et al. Diverse cell surface protein ectodomains are shed by a system sensitive to metalloprotease inhibitors. *J Biol Chem* **271**, 11376-11382 (1996).
21. Hall, K. C. & Blobel, C. P. Interleukin-1 stimulates ADAM17 through a mechanism independent of its cytoplasmic domain or phosphorylation at threonine 735. *PLoS One* **7**, e31600 (2012).
22. Brandl, K. et al. MyD88 signaling in nonhematopoietic cells protects mice against induced colitis by regulating specific EGF receptor ligands. *Proc Natl Acad Sci U S A* **107**, 19967-19972 (2010).
23. Wetzker, R. & Böhmer, F.-D. Transactivation joins multiple tracks to the ERK/MAPK cascade. *Nature reviews Molecular cell biology* **4**, 651-657 (2003).
24. Grieve, A. G. et al. Phosphorylation of iRhom2 at the plasma membrane controls mammalian TACE-dependent inflammatory and growth factor signalling. *Elife* **6**, (2017).
25. Cavadas, M. et al. Phosphorylation of iRhom2 Controls Stimulated Proteolytic Shedding by the Metalloprotease ADAM17/TACE. *Cell Rep* **21**, 745-757 (2017).
26. Dombernowsky, S. L. et al. The sorting protein PACS-2 promotes ErbB signalling by regulating recycling of the metalloproteinase ADAM17. *Nat Commun* **6**, 7518 (2015).

27. Dombernowsky, S. L. et al. Loss of PACS-2 delays regeneration in DSS-induced colitis but does not affect the ApcMin model of colorectal cancer. *Oncotarget* **8**, 108303-108315 (2017).
28. Maney, S. K. et al. Deletions in the cytoplasmic domain of iRhom1 and iRhom2 promote shedding of the TNF receptor by the protease ADAM17. *Sci Signal* **8**, ra109 (2015).
29. Doedens, J. R. & Black, R. A. Stimulation-induced down-regulation of tumor necrosis factor-alpha converting enzyme. *J Biol Chem* **275**, 14598-14607 (2000).
30. Lorenzen, I. et al. Control of ADAM17 activity by regulation of its cellular localisation. *Sci Rep* **6**, 35067 (2016).
31. Hosur, V. et al. Rhbdf2 mutations increase its protein stability and drive EGFR hyperactivation through enhanced secretion of amphiregulin. *Proc Natl Acad Sci U S A* **111**, E2200-9 (2014).
32. Chishti, A. H. et al. et, al (1998). The FERM domain: a unique module involved in the linkage of cytoplasmic proteins to the membrane. *Trends Biochem Sci* **23**, 281-282
33. McClatchey, A. I. ERM proteins at a glance. *J Cell Sci* **127**, 3199-3204 (2014).
34. Fehon, R. G., McClatchey, A. I. & Bretscher, A. Organizing the cell cortex: the role of ERM proteins. *Nat Rev Mol Cell Biol* **11**, 276-287 (2010).
35. Hoover, K. B. & Bryant, P. J. The genetics of the protein 4.1 family: organizers of the membrane and cytoskeleton. *Current opinion in cell biology* **12**, 229-234 (2000).
36. Baines, A. J., Lu, H. C. & Bennett, P. M. The Protein 4.1 family: hub proteins in animals for organizing membrane proteins. *Biochim Biophys Acta* **1838**, 605-619 (2014).
37. Moleirinho, S., Tilston-Lunel, A., Angus, L., Gunn-Moore, F. & Reynolds, P. A. The expanding family of FERM proteins. *Biochem J* **452**, 183-193 (2013).
38. Pearson, M. A., Reczek, D., Bretscher, A. & Karplus, P. A. Structure of the ERM protein moesin reveals the FERM domain fold masked by an extended actin binding tail domain. *Cell* **101**, 259-270 (2000).
39. Pal, S. et al. CCM-3 Promotes C. elegans Germline Development by Regulating Vesicle Trafficking Cytokinesis and Polarity. *Curr Biol* **27**, 868-876 (2017).
40. Kategaya, L. S. et al. Bili inhibits Wnt/beta-catenin signaling by regulating the recruitment of axin to LRP6. *PLoS One* **4**, e6129 (2009).
41. Sahin, U. et al. Distinct roles for ADAM10 and ADAM17 in ectodomain shedding of six EGFR ligands. *J Cell Biol* **164**, 769-779 (2004).
42. Lorenzen, I. et al. Control of ADAM17 activity by regulation of its cellular localisation. *Sci Rep* **6**, 35067 (2016).
43. Zettl, M., Adrain, C., Strisovsky, K., Lastun, V. & Freeman, M. Rhomboid family pseudoproteases use the ER quality control machinery to regulate intercellular signaling. *Cell* **145**, 79-91 (2011).
44. Cullen, P. J. Endosomal sorting and signalling: an emerging role for sorting nexins. *Nature reviews Molecular cell biology* (2008).
45. Böttcher, R. T. et al. Sorting nexin 17 prevents lysosomal degradation of β1 integrins by binding to the β1-integrin tail. *Nat Cell Biol* **14**, 584-592 (2012).
46. Avraham, R. & Yarden, Y. Feedback regulation of EGFR signalling: decision making by early and delayed loops. *Nat Rev Mol Cell Biol* **12**, 104-117 (2011).
47. Wallach, D. The cybernetics of TNF: Old views and newer ones. *Semin Cell Dev Biol* **50**, 105-114 (2016).
48. Vereecke, L., Beyaert, R. & van Loo, G. The ubiquitin-editing enzyme A20 (TNFAIP3) is a central regulator of immunopathology. *Trends Immunol* **30**, 383-391 (2009).
49. Chalaris, A. et al. Critical role of the disintegrin metalloprotease ADAM17 for intestinal inflammation and regeneration in mice. *J Exp Med* **207**, 1617-1624 (2010).
50. Murumkar, P. R., DasGupta, S., Chandani, S. R., Giridhar, R. & Yadav, M. R. Novel TACE inhibitors in drug discovery: a review of patented compounds. *Expert Opin Ther Pat* **20**, 31-57 (2010).
51. Trad, A. et al. Development of sandwich ELISA for detection and quantification of human and murine a disintegrin and metalloproteinase17. *J Immunol Methods* **371**, 91-96 (2011).
52. Luo, W.-W. et al. iRhom2 is essential for innate immunity to DNA viruses by mediating trafficking and stability of the adaptor STING. *Nat Immunol* **17**, 1057-1066 (2016).
53. Henry, C. M. & Martin, S. J. Caspase-8 Acts in a Non-enzymatic Role as a Scaffold for Assembly of a Pro-inflammatory "FADDosome" Complex upon TRAIL Stimulation. *Molecular Cell* **65**, 715-729.e5 (2017).
54. Naviaux, R. K., Costanzi, E., Haas, M. & Verma, I. M. The pCL vector system: rapid production of helper-free, high-titer, recombinant retroviruses. *J Virol* **70**, 5701-5705 (1996).

55. Cong, L. et al. Multiplex genome engineering using CRISPR/Cas systems. *Science* **339**, 819-823 (2013).
56. Wang, H. et al. One-step generation of mice carrying mutations in multiple genes by CRISPR/Cas-mediated genome engineering. *Cell* **153**, 910-918 (2013).
57. Casaca, A., Nóvoa, A. & Mallo, M. Hoxb6 can interfere with somitogenesis in the posterior embryo through a mechanism independent of its rib-promoting activity. *Development* **143**, 437-448 (2016).
58. Hogan, B., Costantini, F. & Lacy, E. *Manipulating the mouse embryo: a laboratory manual* 1986).
59. Bileck, A., Kreutz, D., Muqaku, B., Slany, A. & Gerner, C. Comprehensive assessment of proteins regulated by dexamethasone reveals novel effects in primary human peripheral blood mononuclear cells. *J Proteome Res* **13**, 5989-6000 (2014).
60. Slany, A. et al. Contribution of Human Fibroblasts and Endothelial Cells to the Hallmarks of Inflammation as Determined by Proteome Profiling. *Mol Cell Proteomics* **15**, 1982-1997 (2016).
61. Wiśniewski, J. R., Zougman, A., Nagaraj, N. & Mann, M. Universal sample preparation method for proteome analysis. *Nat Methods* **6**, 359-362 (2009).
62. Sahin, U. et al. A sensitive method to monitor ectodomain shedding of ligands of the epidermal growth factor receptor. *Methods Mol Biol* **327**, 99-113 (2006).
63. Zheng, Y., Schlondorff, J. & Blobel, C. P. Evidence for regulation of the tumor necrosis factor alpha-convertase (TACE) by protein-tyrosine phosphatase PTPH1. *J Biol Chem* **277**, 42463-42470 (2002).
64. Hruz, T. et al. Genevestigator v3: a reference expression database for the meta-analysis of transcriptomes. *Adv Bioinformatics* **2008**, 420747 (2008).

Figure 1, Oikonomidi *et al.*

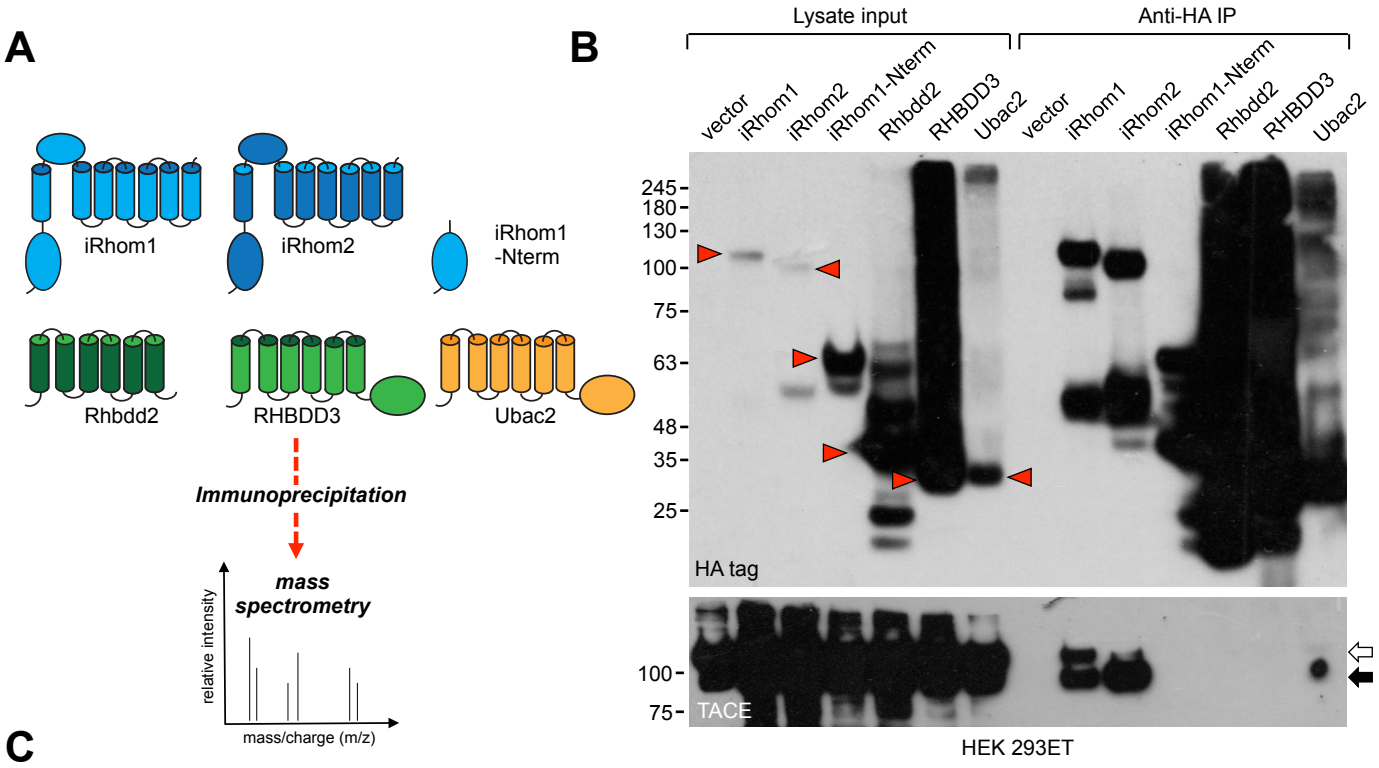

C

	vector	iRhom1	iRhom2	iRhom1-Nterm	Rhbdd2	RHBDD3	Ubac2
peptides	-	MDGTEGSAGQPGPAER	-	-	-	-	-
	-	-	-	QWPELLLR	-	-	-
	-	FTSAPDDDVAMDEPFLQFR	FTSAPDDDVAMDEPFLQFR	FTSAPDDDVAMDEPFLQFR	-	-	-
	-	ELQIHDEEVLR	ELQIHDEEVLR	ELQIHDEEVLR	-	-	-
	-	YPCDVEDCEALGALVCR	-	YPCDVEDCEALGALVCR	-	-	-
	-	LDSFLPAHLCK	-	-	-	-	-
	-	AGPGEQGLLNAYR	AGPGEQGLLNAYR	AGPGEQGLLNAYR	-	-	-
	-	-	-	QVQEVSSDGGCEAALGTHYR	-	-	-
	-	-	-	HVLLGLR	-	-	-
	-	IQHLSTIDYVEDGK	-	IQHLSTIDYVEDGK	-	-	-
	-	QLSLGQGSYTVVQPGDSLEQG	-	-	-	-	-
% coverage	0%	26.29%	9.27%	23.49%	0%	0%	0%

Total coverage of FRMD8/iTAP sequence:

MDGTEGSAGQ PGPAERSHRS SVSSVGARAA DVLVYLADDT VVPLAVENLP SLSAHELHRA VREVLQLPDI
ALDVFALWLV SPLLEVQLKP KHQPYKLGR**Q WPELLLRFTS APDDDVAMDE PFLQFR**RNVF FPKRR**ELQIH**
DEEVLRLLYE EAKGNVLAAR **YPCDVEDCEA LGALVCR**VQL GPYQPGRPAA CDLREK**LDSF LPAHLCK**RGQ
SLFAALRGRG AR**AGPGEQGL LNAYRQVQEV SSDGGCEAAL GTHYR**AYLLK CHELPFYGCA FFHGEVDKPA
QGFLHRGGRK PVSVAISLEG VHVIDSREK**H VLLGLR**FQEL SWDHTSPEEE EPILWLEFDG DSEGTPVNKL
LKIYSKQAEL MSSLIEYCIE LSQAAEPAGP QDSATGSPSD PSSSLAPVQR PKLRRQGSVV SSR**IQHLSTI**
DYVEDGKGIR RVKPKRTTSF FSR**QLSLGQG SYTVVQPGDS LEQG**

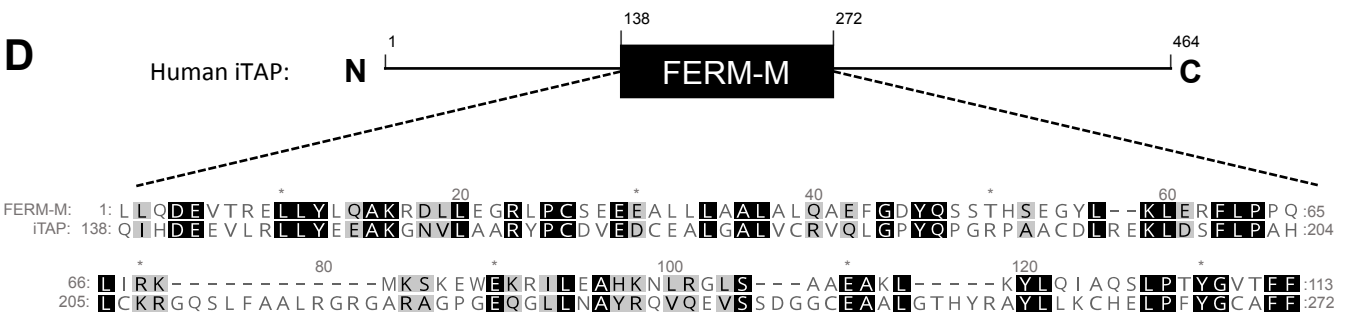

Figure 1—figure supplement 1, Oikonomidi *et al.*

A

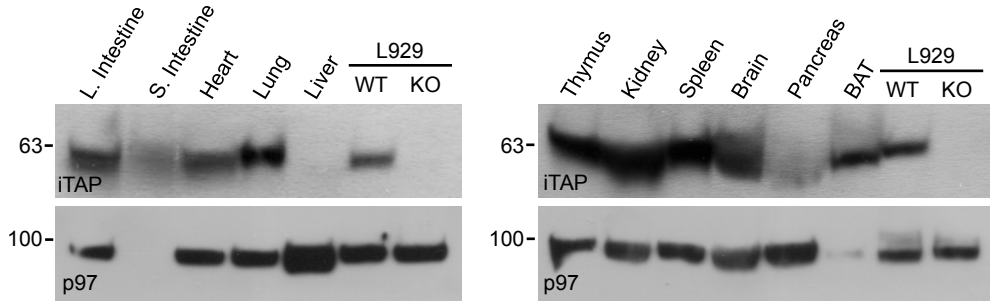

B

Figure 2, Oikonomidi *et al.*

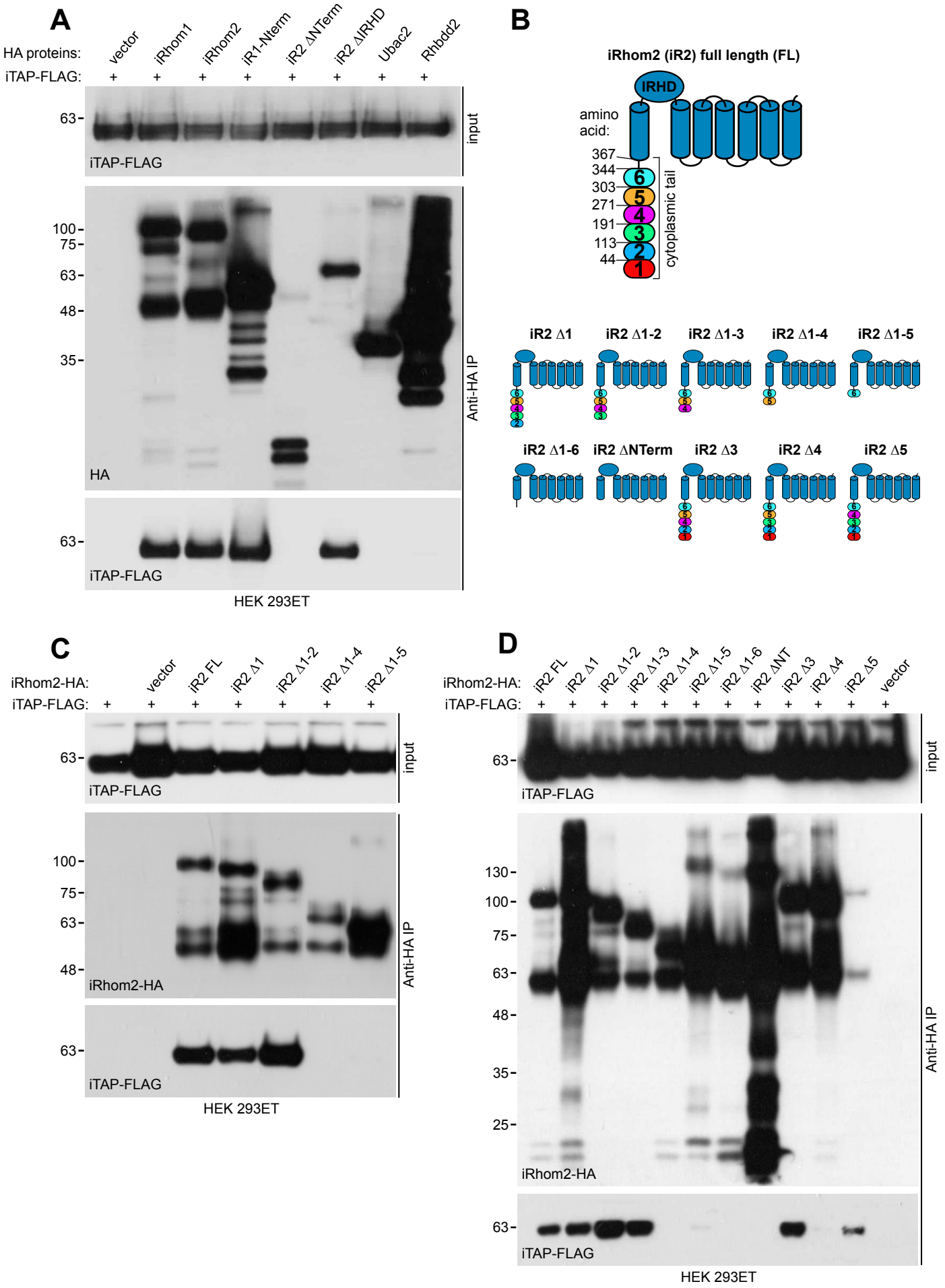

Figure 2—figure supplement 1, Oikonomidi *et al.*

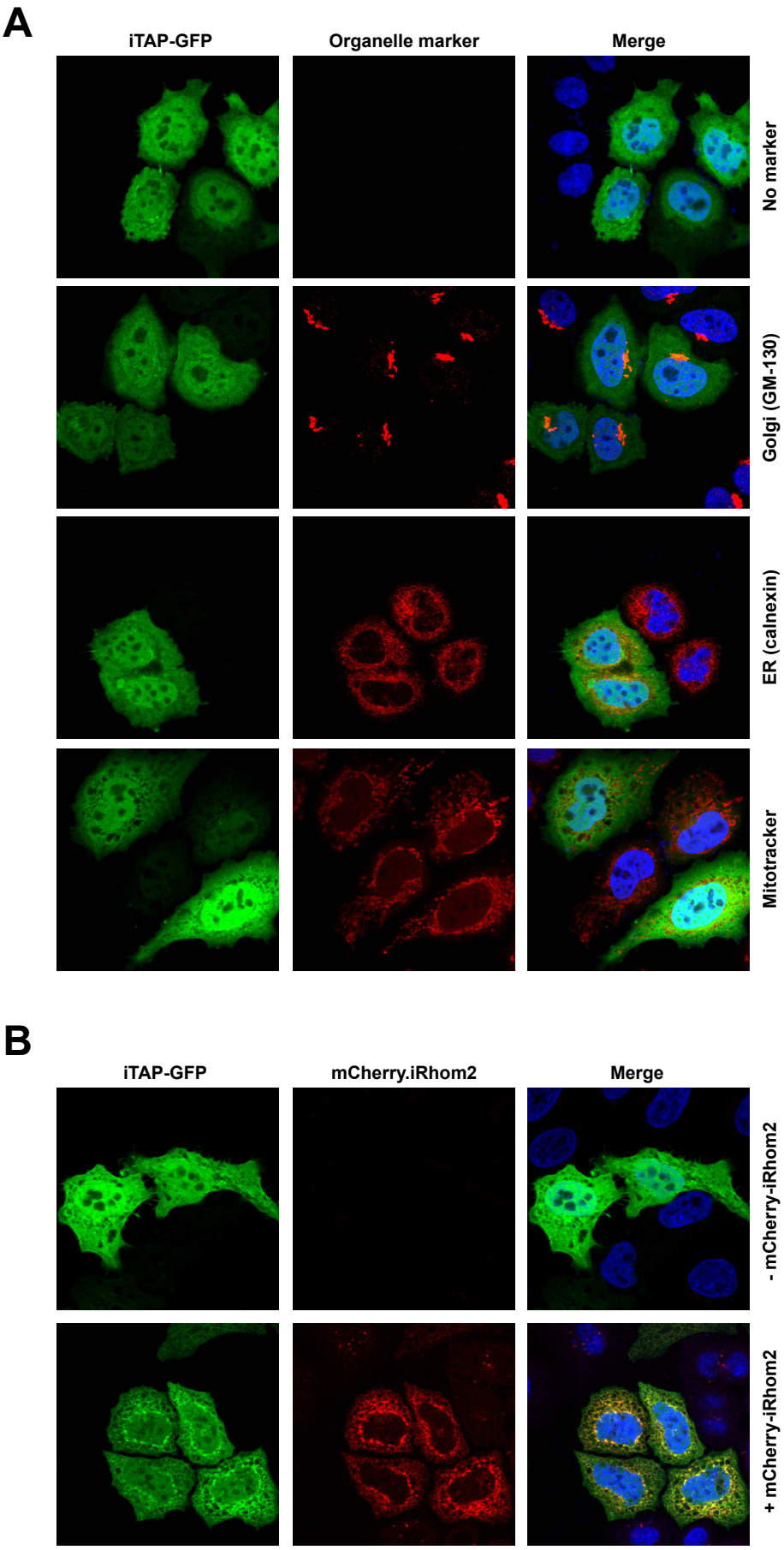

Figure 3, Oikonomidi *et al.*

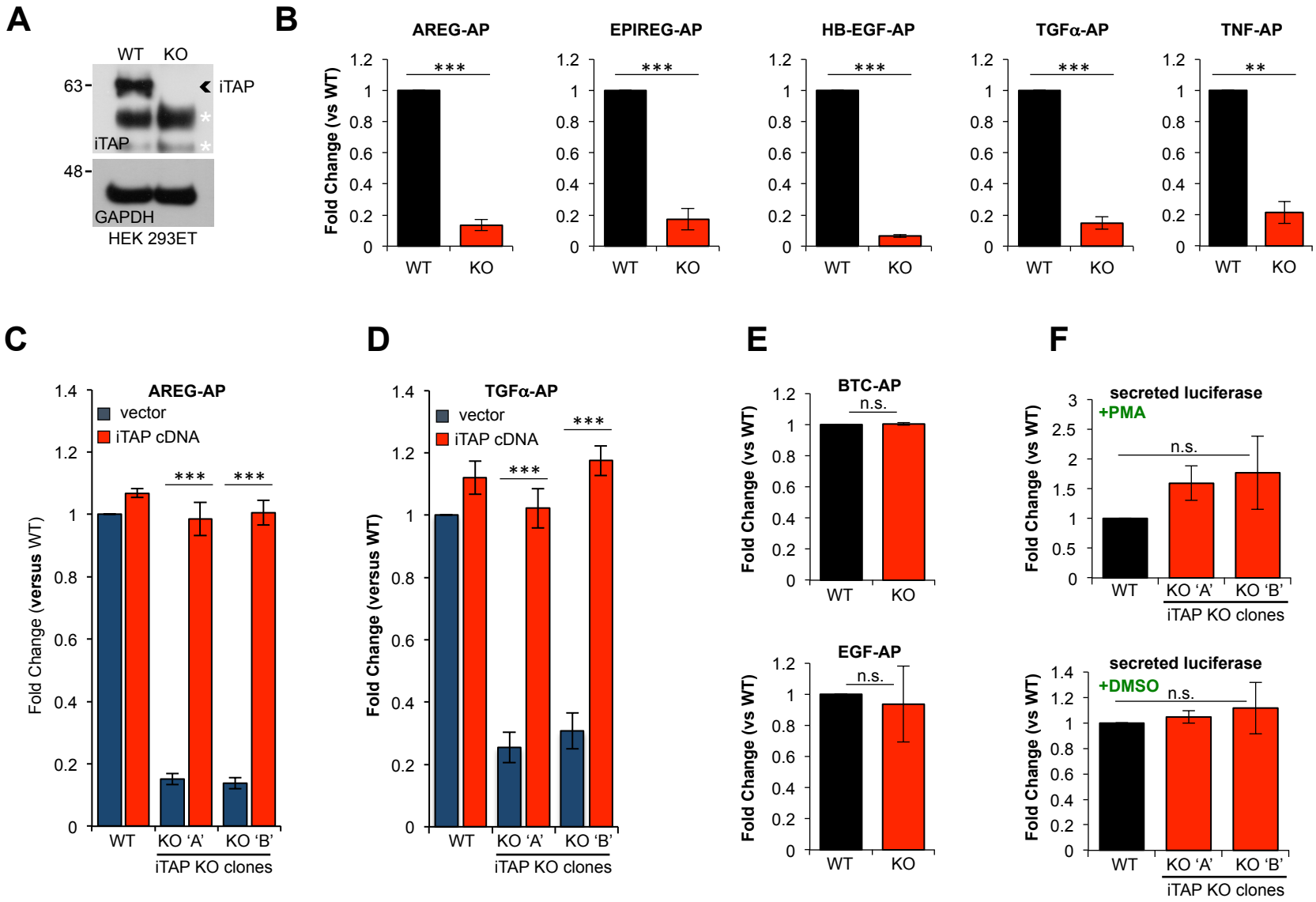

Figure 3—figure supplement 1, Oikonomidi *et al.*

A

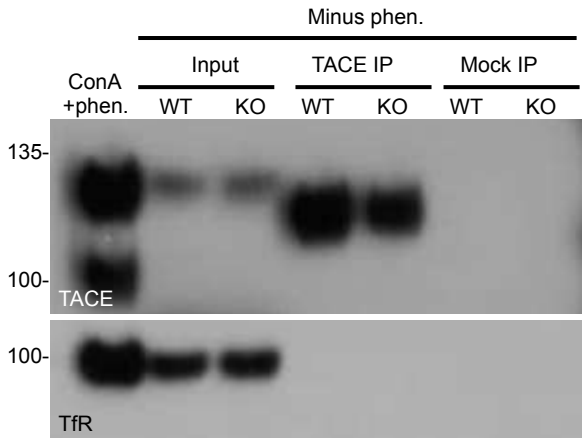

B

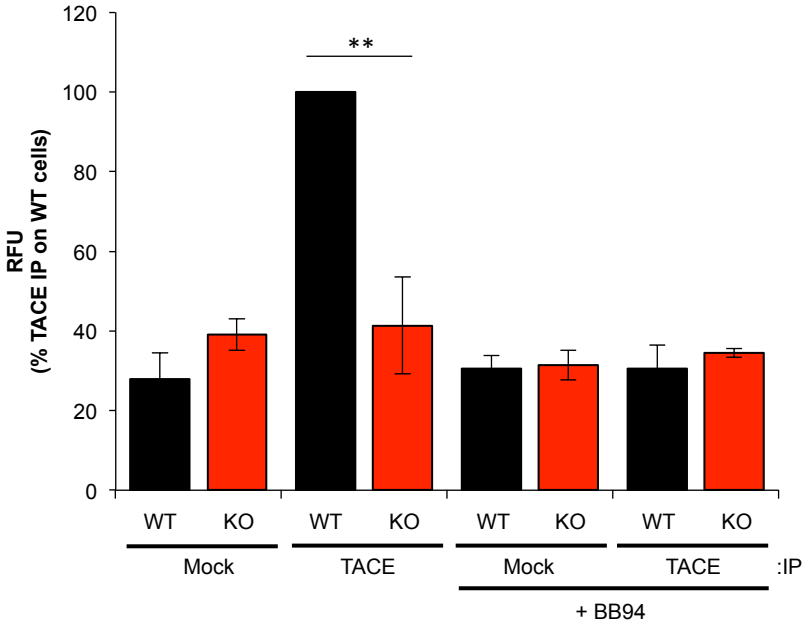

Figure 4, Oikonomidi *et al.*

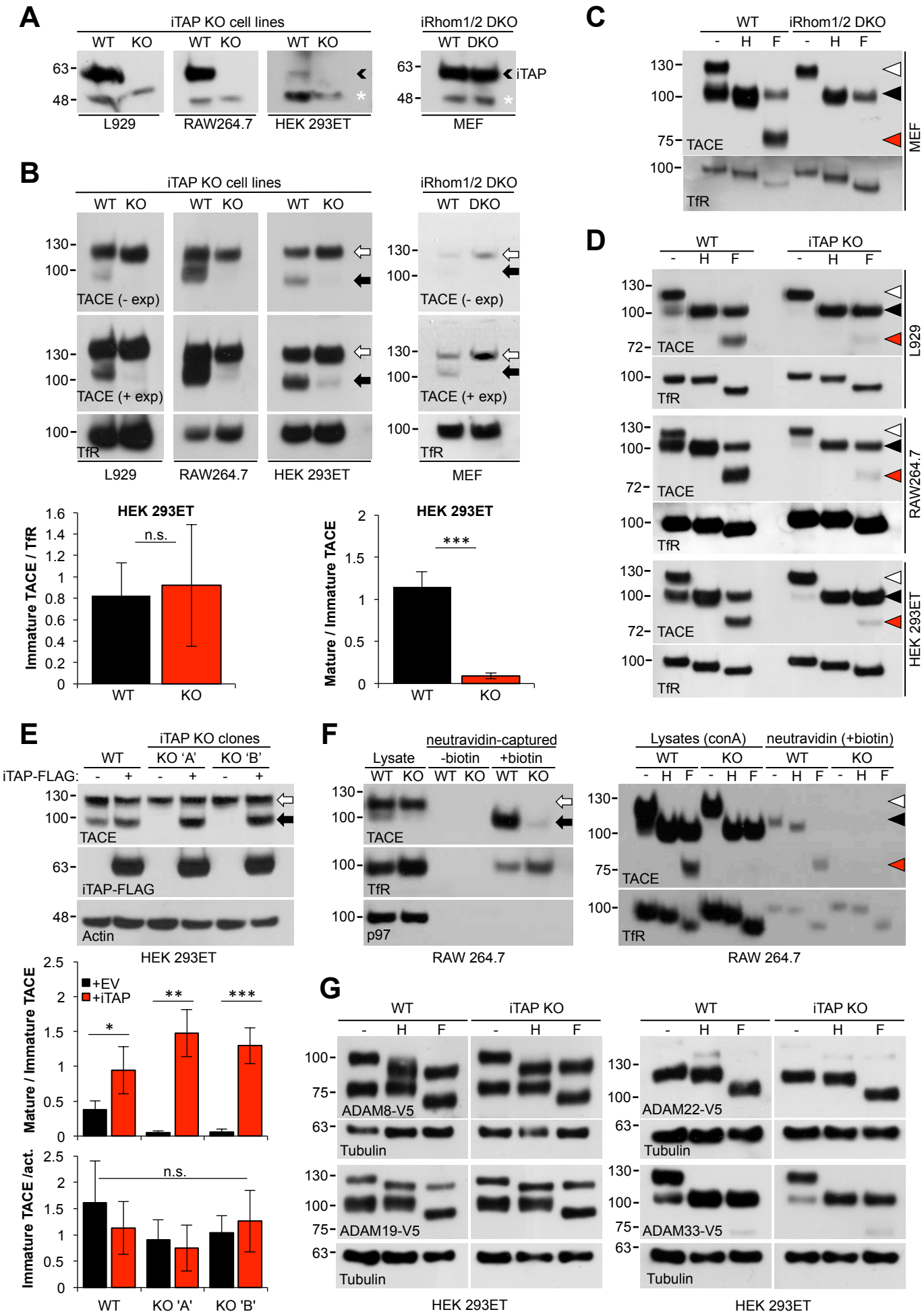

Figure 5, Oikonomidi *et al.*

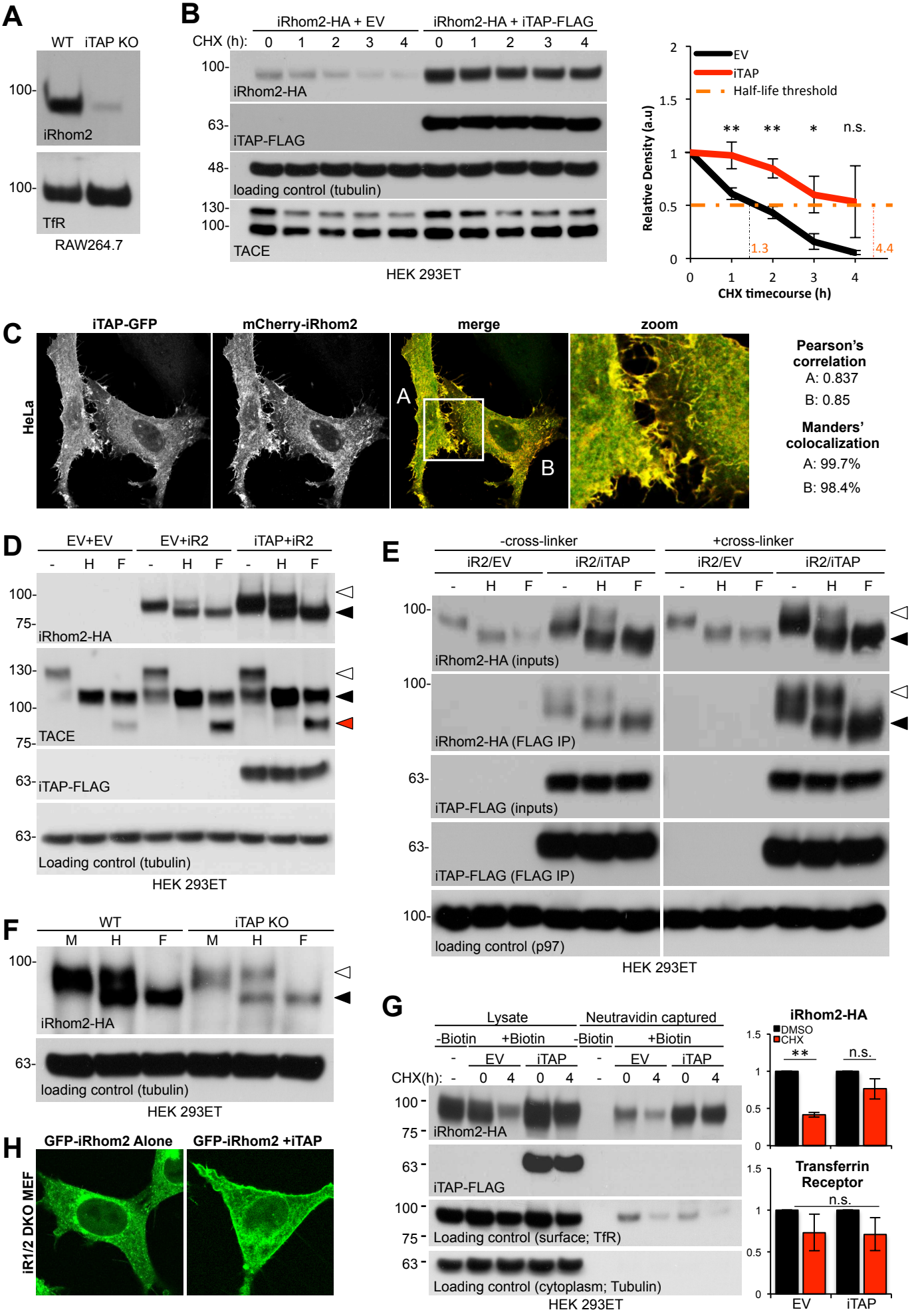

Figure 5—figure supplement 1, Oikonomidi *et al.*

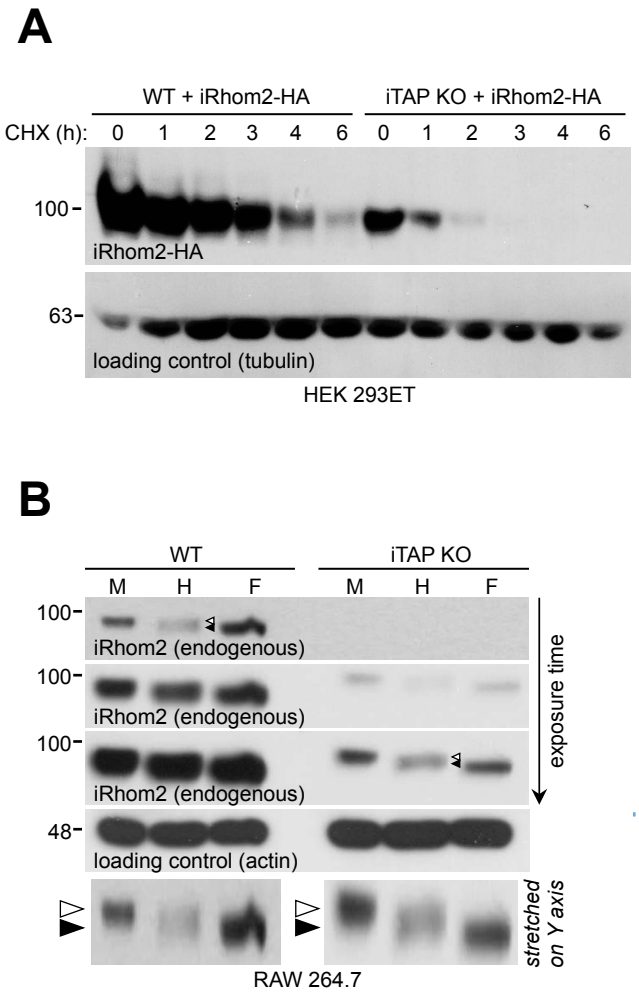

Figure 6, Oikonomidi *et al.*

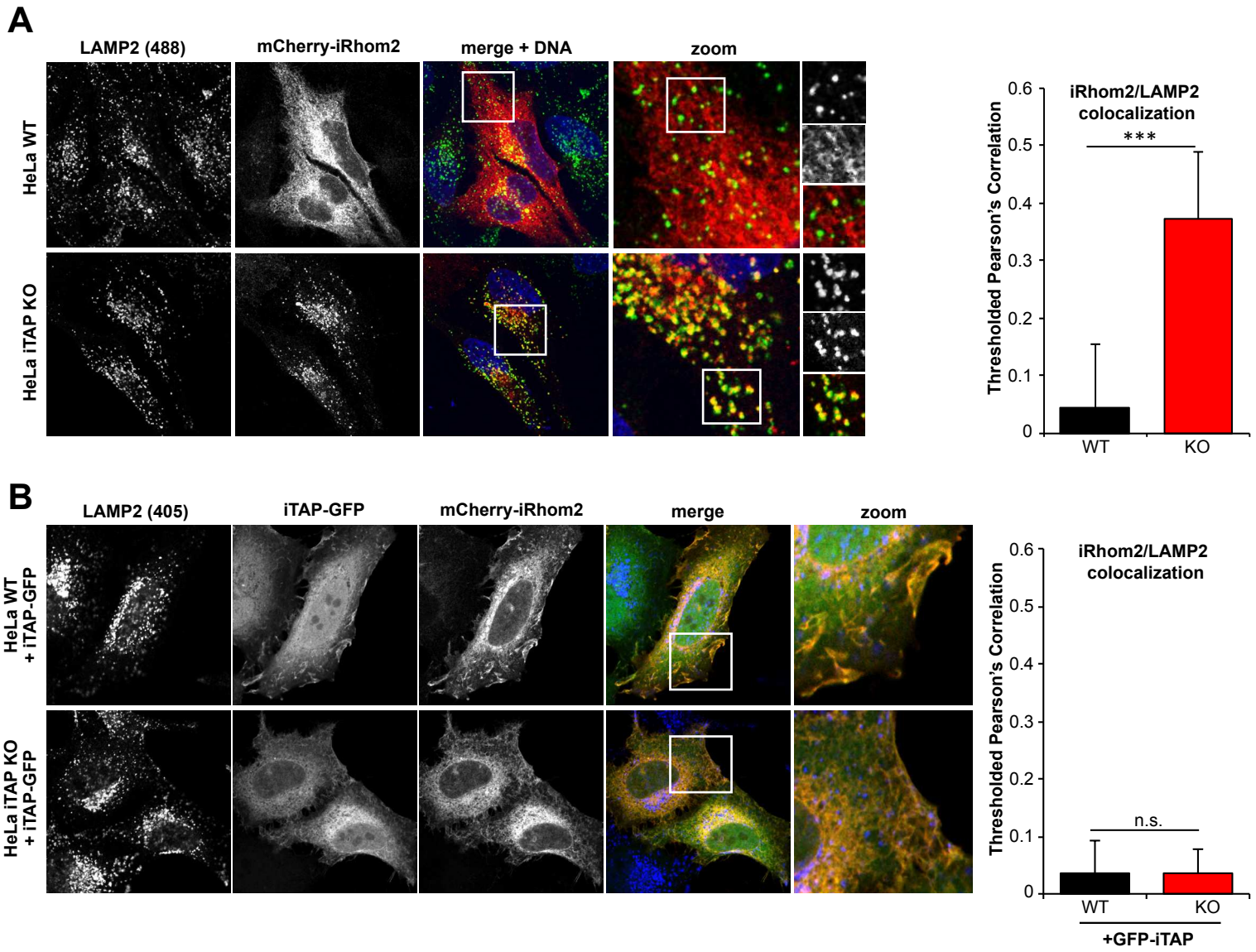

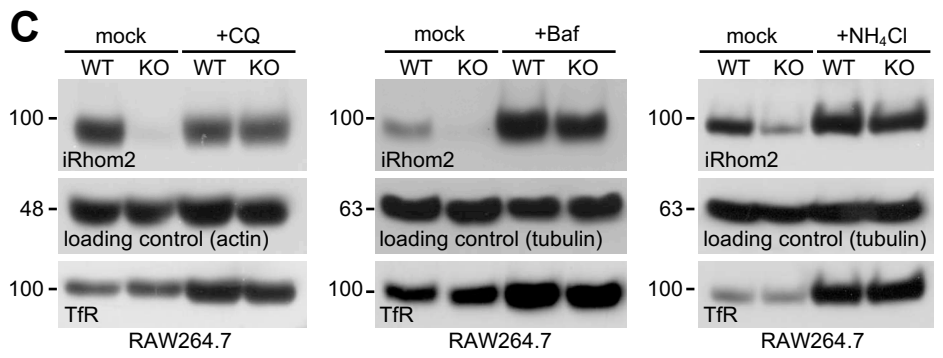

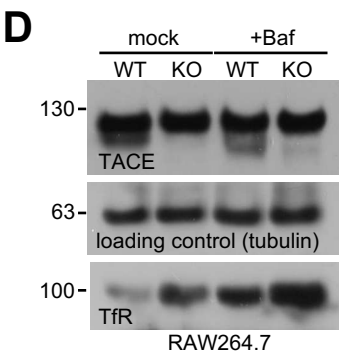

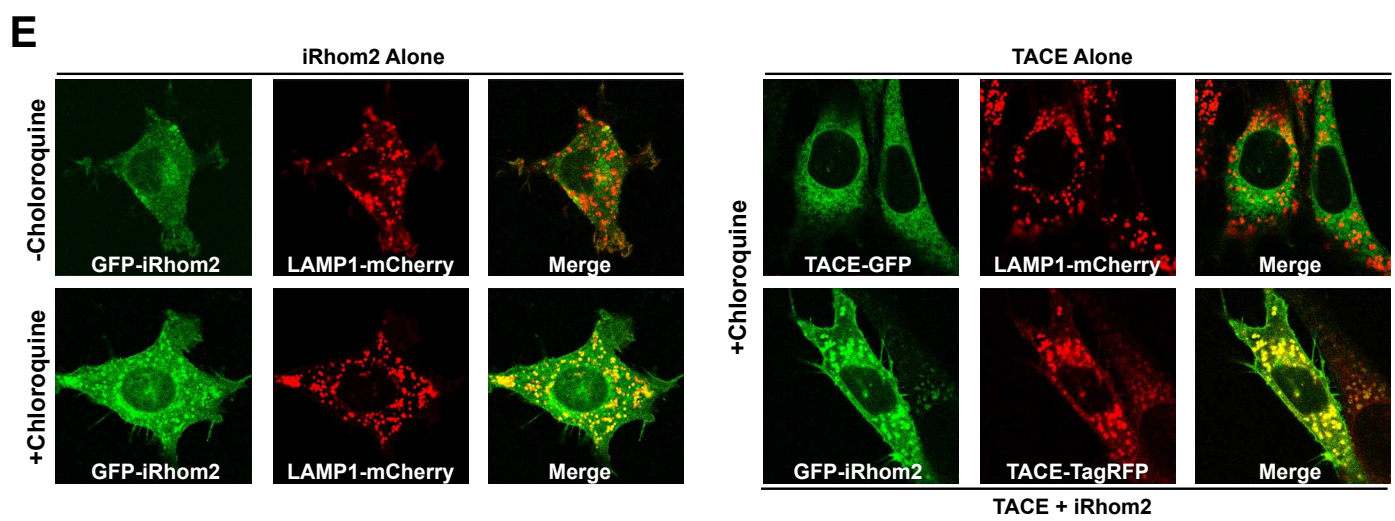

Figure 6—figure supplement 1, Oikonomidi *et al.*

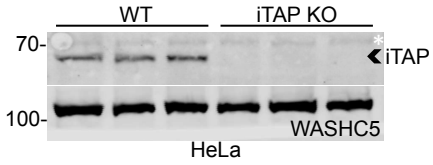

Figure 7, Oikonomidi *et al.*

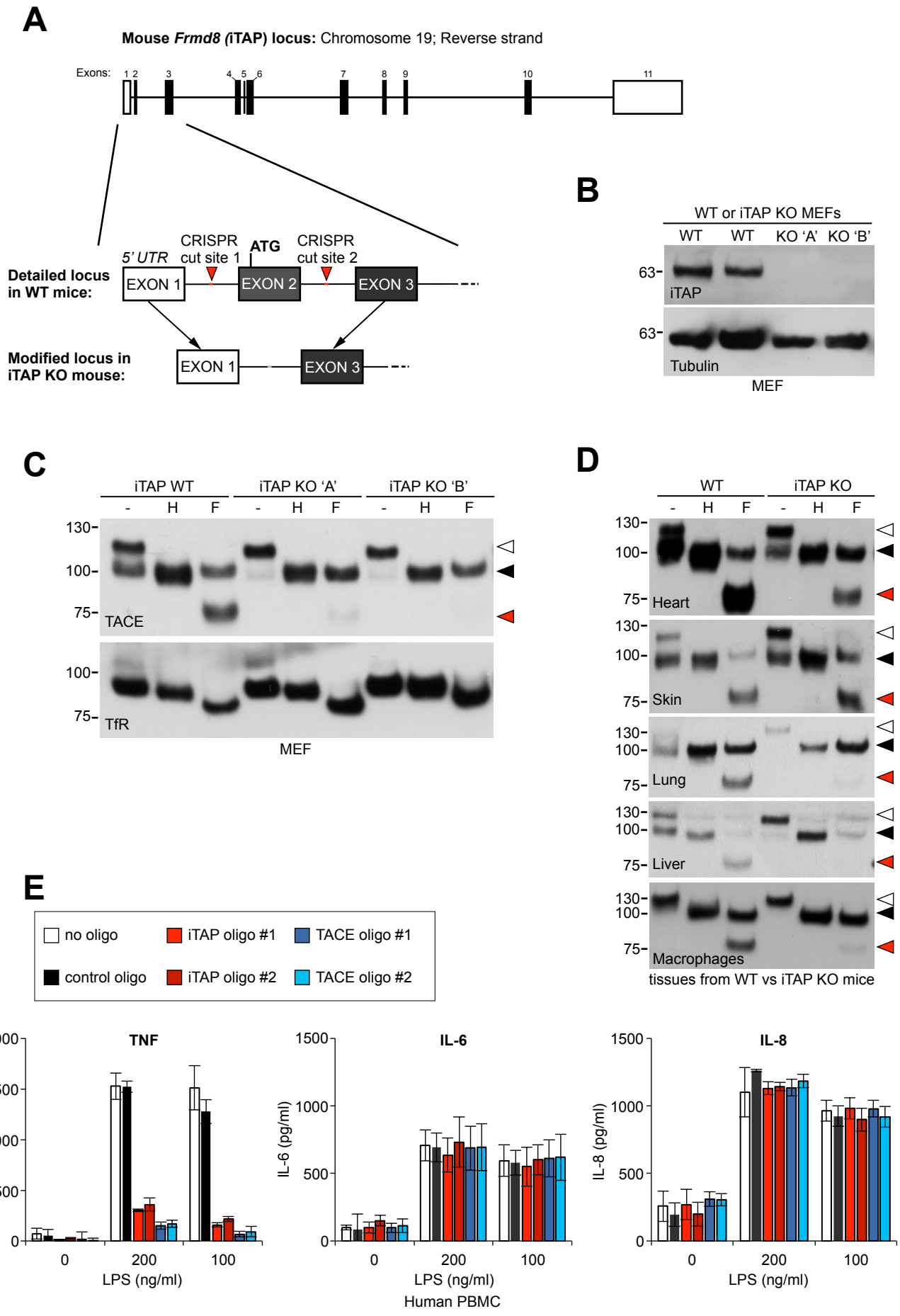

Figure 7—figure supplement 1, Oikonomidi *et al.*

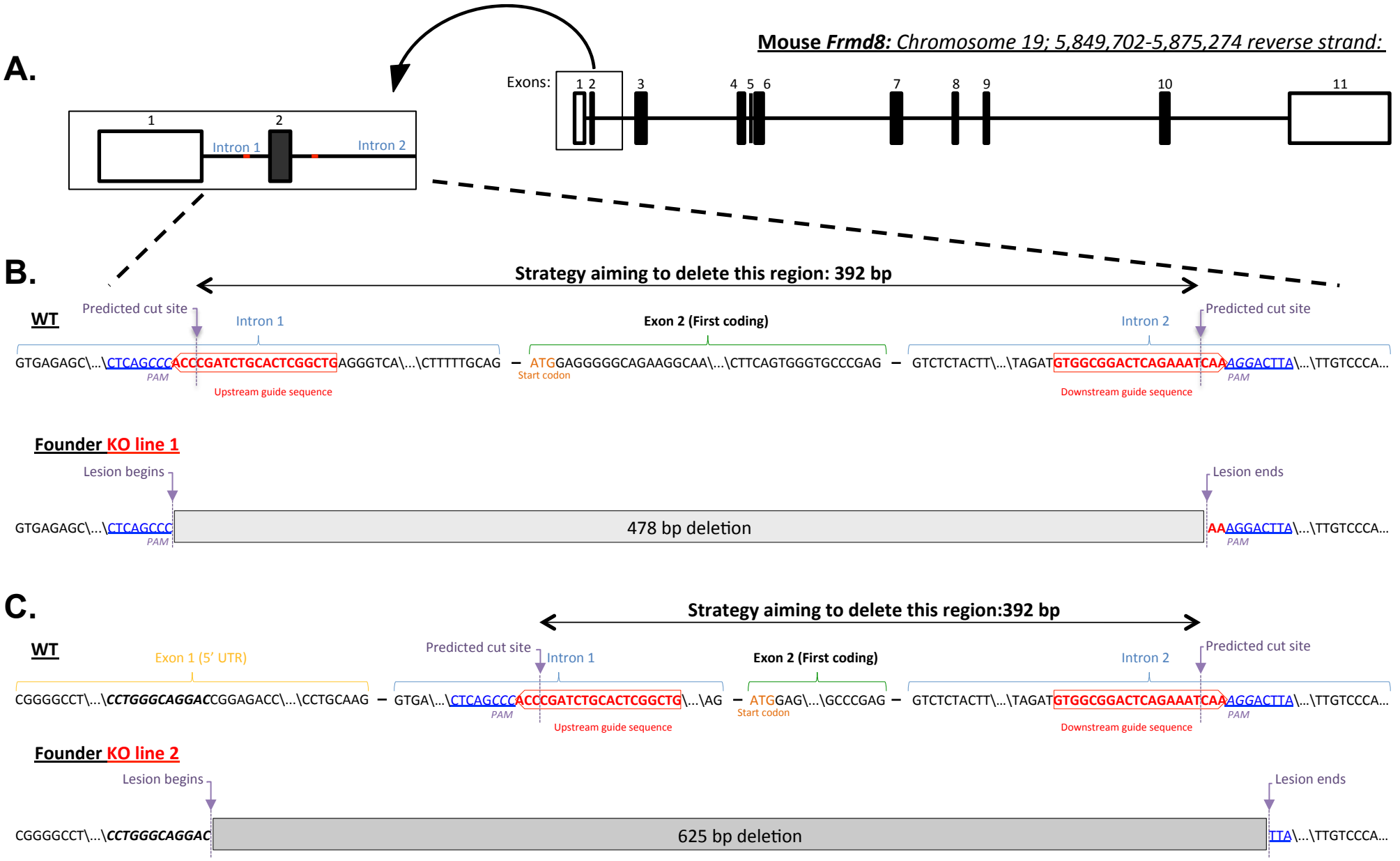

Figure 8, Oikonomidi *et al.*

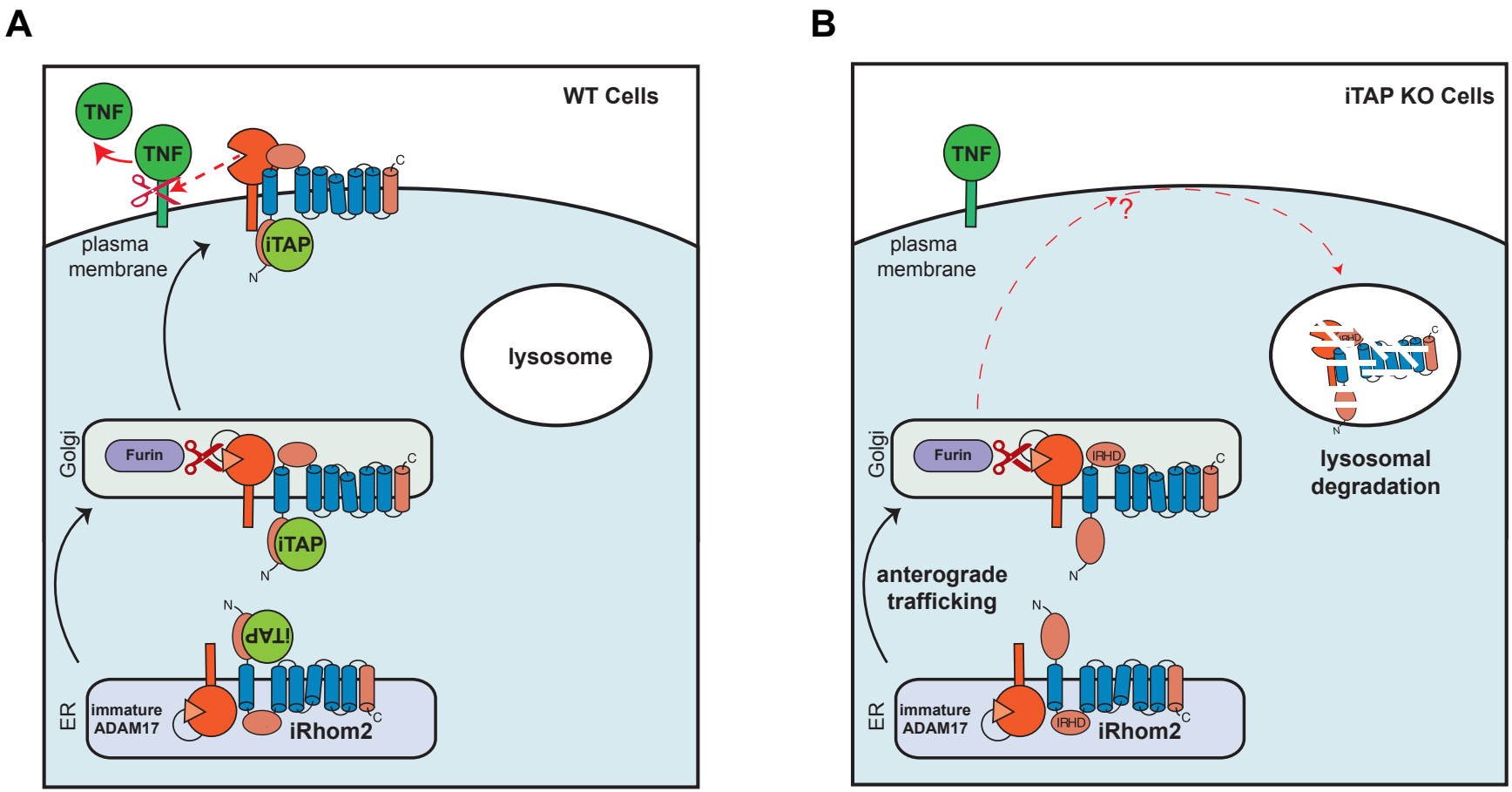

Figure 8—figure supplement 1, Oikonomidi *et al.*